catalysts

MDPI

Review

Synthesis and Surface Modification of TiO_2-Based Photocatalysts for the Conversion of CO_2

Samar Al Jitan [1,2], Giovanni Palmisano [1,2,*] and Corrado Garlisi [1,2]

[1] Department of Chemical Engineering, Khalifa University, Abu Dhabi P.O. Box 127788, UAE; samar.aljitan@ku.ac.ae (S.A.J.); corrado.garlisi@ku.ac.ae (C.G.)

[2] Research and Innovation Center on CO_2 and H_2 (RICH Center), Khalifa University, Abu Dhabi P.O. Box 127788, UAE

* Correspondence: giovanni.palmisano@ku.ac.ae; Tel.: +971-02-810-9246

Received: 12 December 2019; Accepted: 23 January 2020; Published: 14 February 2020

Abstract: Among all greenhouse gases, CO_2 is considered the most potent and the largest contributor to global warming. In this review, photocatalysis is presented as a promising technology to address the current global concern of industrial CO_2 emissions. Photocatalysis utilizes a semiconductor material under renewable solar energy to reduce CO_2 into an array of high-value fuels including methane, methanol, formaldehyde and formic acid. Herein, the kinetic and thermodynamic principles of CO_2 photoreduction are thoroughly discussed and the CO_2 reduction mechanism and pathways are described. Methods to enhance the adsorption of CO_2 on the surface of semiconductors are also presented. Due to its efficient photoactivity, high stability, low cost, and safety, the semiconductor TiO_2 is currently being widely investigated for its photocatalytic ability in reducing CO_2 when suitably modified. The recent TiO_2 synthesis and modification strategies that may be employed to enhance the efficiency of the CO_2 photoreduction process are described. These modification techniques, including metal deposition, metal/non-metal doping, carbon-based material loading, semiconductor heterostructures, and dispersion on high surface area supports, aim to improve the light absorption, charge separation, and active surface of TiO_2 in addition to increasing product yield and selectivity.

Keywords: photocatalytic reduction; CO_2; TiO_2 photocatalysts; surface modification; solar fuel

1. Introduction

The global emission of greenhouse gases, such as CO_2, continues to rise by ~3% each year [1]. Higher atmospheric concentrations of greenhouse gases lead to surface warming of the land and oceans [2]. According to computational results based on climate models, the average global value of the temperature rise of +2 °C will be surpassed when the concentration of CO_2 reaches 550 ppm [1]. If current trends are kept, the CO_2 concentration will reach this threshold value by 2050. In addition to warming the Earth, CO_2 emissions have increased the ocean's acidity. Thirty million of the 90 million tons of CO_2 discharged each day end up in the oceans as carbonic acid, lowering the ocean's pH level [3]. Both the increased temperatures and the higher acidity of the ocean have initiated a set of other impacts including the melting of glaciers, rising sea levels, deeper and longer droughts, more and larger forest fires, migration of tropical diseases, accelerated extinction rates, increased destructive power of tropical storms, and increasingly large downpours of rain and snow [3,4]. Natural processes can potentially remove most of the CO_2 that human activities are adding to the atmosphere; however, these processes operate very slowly and will take too long to prevent rapid climate change and its impacts [2].

Three theoretical approaches have been widely suggested for solving the climate problem: (1) direct reduction of CO_2 emissions by changing industrial and urban processes and habits, (2) CO_2

capture and storage (CCS), and (3) CO_2 capture and utilization (CCU). Due to the increasing population rate and the increasing demand for high-quality life, the direct reduction of CO_2 emissions seems infeasible [5]. To keep up with energy needs of a growing population, governments are compelled to continue with their current industrial activities despite the large amounts of resulting greenhouse gas emissions. Carbon capture and sequestration (CCS) is considered to be a very promising solution to removing excess CO_2 from the atmosphere. The idea behind CCS lies in storing large quantities of captured CO_2 in underground geological formations. The stored CO_2 may be used for recovering oil and gas from partly exploited fields, thus giving an economic value to CO_2 [6]. The two major issues associated with CCS are cost and storage. The high cost of CCS is due to the large amounts of energy required to separate CO_2 from the emission stream. It is estimated that this separation process could account for 70–90% of the total operating cost of CCS [7]. Also, the storage of CO_2 is considered challenging due to the large amounts of CO_2 that needs to be stored and the risk of leakage [2]. Although CCS technologies may appear to be very promising in removing excess CO_2 from the atmosphere, they are expensive, energy-intensive, and require large capital investment for industrial application [8].

To make CCS technologies more economically feasible, carbon capture and utilization (CCU) technologies have emerged as a feasible and promising technique that can complement the storage of huge quantities of CO_2 in geological and ocean formations. Industrial applications of CO_2 are present in numerous sectors including chemical, oil and gas, energy, pulp and paper, steel, food, and pharmaceuticals [9]. Currently, the commercial CCU technologies use CO_2 for enhanced oil recovery (EOR) applications. The use of CO_2 as a raw input material in the chemical industry is limited to a few processes such as the production of salicylic acid, urea and polycarbonates [8,10]. Recently, new research is looking into converting the captured CO_2 into valuable products including chemicals, polymers and fuel. It is estimated that 5 to 10% of the total CO_2 emissions may be utilized for the synthesis of value-added products [11]. The specific application of converting CO_2 into fuel is being actively studied by researches and is showing great promise for future industrial applications. A wide variety of fuels, including methanol, ethanol, methane, dimethyl ether, formic acid, petroleum-equivalent fuels, and others may be produced through different CO_2 conversion processes. However, these conversion processes produce large quantities of CO_2 and will therefore increase the concentration of CO_2 in the atmosphere instead of reducing it [11,12]. Thus, to stay within the targeted goal of decreasing CO_2 emissions, low-carbon energy sources, such as renewable resources, must be used as the primary energy input in the CO_2-to-fuels conversion process. Other drawbacks of CO_2-to-fuels conversion processes include intensive energy requirements and low energy conversion efficiency [12]. The main methods of CO_2 conversion are thermochemical [13–15], electrochemical [12,13], biological [16–18], and photocatalytic [19–23].

Photocatalysis is considered to be a promising method for the conversion of CO_2 into valuable products, such as methane, hydrogen, methanol, formaldehyde, ethanol, and higher hydrocarbons [6,19]. One major advantage of photocatalysis over other conversion methods is that it can take place at room temperature and under atmospheric pressure conditions [19]. In addition to that, it utilizes a renewable and sustainable form of energy, namely solar energy, for the conversion of CO_2. Note that, unlike conventional processes, the photoreduction of CO_2 does not increase net CO_2 emissions or consume additional energy [23]. Despite the intensive research, the photocatalytic reduction of CO_2 is still considered inefficient. This is mainly due to the absence of scalable reactor designs able to simultaneously introduce reactants, photons, and visible light-responsive catalysts to produce specific fuels in significant quantities [23]. The main challenge in developing an economically feasible process for the photocatalytic conversion of CO_2 is finding a suitable catalyst [24]. The most common type of catalysts used in the photocatalytic conversion of CO_2 are the inexpensive and naturally abundant transition-metal oxides, such as titanium dioxide (TiO_2). TiO_2 is one of the most widely used and commonly investigated semiconductors for photocatalytic applications [25]. This is attributed to its low toxicity, low cost, high efficiency, and high stability. Other several types of metal oxide semiconductors,

including zirconium oxide, gallium oxide and thallium oxide, have also been investigated for their use in the photocatalytic reduction of CO_2 [25]. The poor light absorption and the low product selectivity of these photocatalysts pose a challenge for researchers aiming to efficiently reduce CO_2 [26]. Currently, the development of new, stable, inexpensive, abundant, nontoxic, selective, and visible light-responsive photocatalysts is being actively investigated [19,27]. In this regard, some state-of-the-art photocatalysts, such are perovskite oxides and III-V semiconductors, have shown some great promise in driving the photocatalytic reduction of CO_2 specifically under direct sunlight. Perovskite oxides exhibit interesting compositional flexibility that allows for precise band gap tuning and defect engineering [28]. On the other hand, III-V semiconductors can easily meet the thermodynamic requirements of CO_2 reduction to CO due to their higher (less positive) conduction band when compared to that of other metal oxide semiconductors [29]. Nonetheless, the current photocatalytic efficiency of perovskite oxides and III-V semiconductors is too low for practical CO_2 reduction applications. Furthermore, their low selectivity and high instability have urged researches to continue with their investigations on TiO_2-based photocatalysts for the reduction of CO_2 [28].

Besides enhanced photocatalysts, researchers have been also coupling photocatalysis with other CO_2 conversion methods aiming at improving the process efficiency. For instance, in a study proposed by Zhang et al. [30], a photo-thermochemical process was used for the reduction of CO_2. Combining both processes together allowed for the utilization of both solar and thermal energy. The major limitation of thermochemical conversion techniques is the high temperature (>1273 K) step required to reduce the metal oxide catalyst and create an oxide vacancy. In the photo-thermochemical process, this step is replaced by photocatalysis where UV light is used instead of high temperatures to form vacant sites. Next, the temperature needs to be only slightly raised (573–873 K) to accelerate the dissociation of CO_2 to CO. Electrocatalysis is another CO_2 conversion method that has been coupled with photocatalysis. As previously mentioned in this work, photocatalysts with outstanding structural and optical properties need to be developed for an efficient CO_2 photoreduction process. From a thermodynamic perspective, these photocatalysts must possess favorable band gap energies for CO_2 reduction. In photo-electrocatalysis, this limitation may be overcome if an appropriate external bias is applied to the system [31]. Therefore, a broader range of photocatalysts with lower thermodynamic restrictions can be used for the reduction of CO_2. Halmann [32] was the first to report the successful photo-electrocatalytic conversion of CO_2 into formic acid, formaldehyde, and methanol.

In this review, the current advances on CO_2 photoreduction over TiO_2-based catalysts are critically discussed. The photocatalytic mechanism of CO_2 reduction has been explained particularly in the case when water is used as a reductant. Furthermore, the various modification techniques of TiO_2, including metal deposition, metal/non-metal doping, carbon-based material loading, formation of semiconductor heterostructures, and dispersion on high surface area supports, have been summarized. Although a number of review articles [33–35] have highlighted the possible surface modifications of TiO_2 photocatalysts, this paper provides emphasis on modification techniques that will specifically enhance the CO_2 photoreduction efficiency of TiO_2 photocatalysts. Future directions toward efficient photocatalytic systems for the reduction of CO_2 have been also presented.

2. Photocatalytic Conversion of CO_2: Thermodynamics and Kinetics

In the photocatalytic approach, semiconductors irradiated by UV or visible light are used for the reduction of CO_2. As can be seen in Figure 1, the light energy ($h\nu$) absorbed by the photocatalyst is used to produce electron–hole pairs, which are generated when that energy is equal or greater than the band gap energy (E_g) of the photocatalyst. Only then will the electrons (e^-) be promoted from the valence band (VB) to the conduction band (CB) of the semiconducting material, simultaneously creating a hole (h^+) at the VB [20]. The e^- and h^+ are then transferred to active redox species present across the photocatalytic interface in order to participate in the conversion process [26].

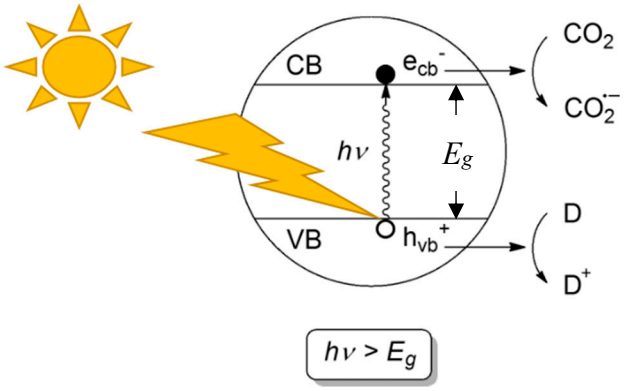

Figure 1. Generation of an electron–hole pair in a photocatalyst. Reproduced from work in [20]. Copyright 2011 Royal Society of Chemistry.

The photocatalytic reduction of CO_2 into value-added products involves radical-chain reactions that form cation, anion, and electrically neutral or charged radicals. These radicals are produced as a result of the reaction with photogenerated electrons and holes between the metal oxide photocatalyst and the reactants [26,36]. As CO_2 will be reduced, the presence of a co-reagent, or an electron donor, that will be simultaneously oxidized, is necessary [37]. A sacrificial donor (D), usually water, is oxidized by the photogenerated holes in the valence band, while the electrons in the conduction band reduce CO_2 [38]. Hydroxyl groups present on the surface of the photocatalyst might also be oxidized by the holes [39]. The end products of the photocatalytic reduction of CO_2 depend on both the redox potential (thermodynamics), and surface electron density and photoadsorption/photodesorption thermodynamics and kinetics [40].

The overall efficiency of the photocatalytic reduction of CO_2 is governed by the effectiveness of three processes: the photogeneration of the electron/hole pair, the interfacial transfer of electrons between the photocatalyst surface and the adsorbed CO_2, and the conversion of redox species to valuable products [20]. The features of the photocatalyst, the energy of light, and the concentration of reactants are all factors that greatly influence the reaction rate of the photocatalytic process. Other important parameters include pH (when the reaction takes place in water), which affects the charge of the photocatalytic surface, and temperature, which impacts the collision frequency between the reactants and the photocatalyst [21]. Moreover, the surface of the photocatalyst must be thoroughly cleaned prior to any photocatalytic test. Otherwise, carbon-containing species, resulting from the synthesis procedure, will be present on the photocatalyst's surface and will contribute to product formation. Dilla et al. [41] developed an efficient photocatalytic cleaning step that may be performed right before the start of the CO_2 photoreduction test. Herein, humid helium is flushed through the reactor under light irradiation. The cleaning progress is then monitored and, as soon as the concentration of products from the cleaning reaction is low, CO_2 is fed into the reactor. This method not only ensures a clean photocatalytic surface but also rids the reactor from any trace hydrocarbon contaminants that might be present inside.

If the participating species are adsorbed on the semiconductor surface, then the photocatalytic process will certainly be more efficient due to the decrease in activation energy and increase in substrate concentration near reactive sites. When CO_2 adsorbs onto the photocatalyst surface, its structure transforms from linear to the more reactive bent form (Figure 2). More specifically, the carbon atom of CO_2 binds to a surface oxygen site, while the oxygen atom binds to the surface metal center of the metal oxide [42]. As a result of the structural transformation, the lowest unoccupied molecular orbital (LUMO) level of the metal oxide decreases lowering its activation energy [39]. However, density functional theory (DFT) calculations performed by Sorescu et al. [43] demonstrated that CO_2 preferentially binds to the metal oxide surface in a linear geometry. This is most probably due to the low binding energy (−46 kJ/mol) associated with the linear configuration, the considerable energy

required to bend CO_2 (38.6 kcal/mol) and the significant deformation the metal oxide surface undergoes when binding to bent CO_2 [42,43].

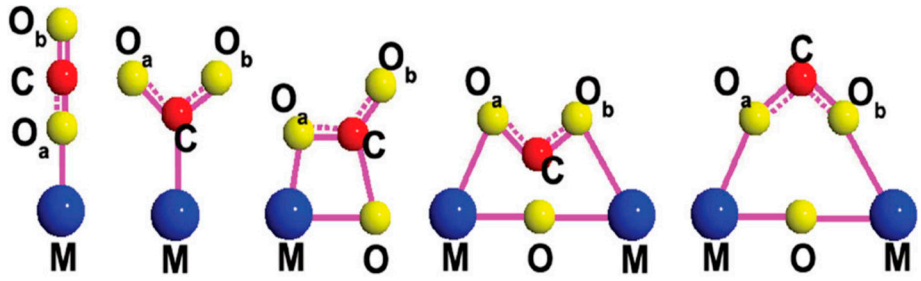

Figure 2. Five possible CO_2 adsorption configuration models on metal oxide semiconductors. M: Metal C: Carbon O: Oxygen. Reproduced from work in [44]. Copyright 2014 Wiley-VCH.

To enhance the adsorption of CO_2, basic sites and/or micropores must be introduced on the surface of the photocatalyst. The introduction of sites that can store electrons and acid sites that can stabilize the species derived from CO_2 must also be considered [37]. Therefore, researchers have to focus on developing such complex photocatalysts with a combination of acidic and basic sites. Additionally, the adsorption of CO_2 could also be improved by synthesizing metal-oxide photocatalysts with oxygen vacancy sites. These vacancies may then be filled by the oxygen atoms of CO_2 promoting the adsorption of the latter [45]. The generation of an unexpected attraction between the oxygen vacancy and CO_2 subsequently lowers the reactive barrier [44].

A large and negative reduction potential ($E = -1.90$ V) is required for the single electron reaction that coverts CO_2 to $CO_2^{\bullet-}$ [46]:

$$CO_2 + e^- \rightarrow CO_2^{\bullet-}, \quad (1)$$

This reaction is thermodynamically unfavorable due to the high stability of CO_2 and the large amount of energy needed to change the geometrical configuration of CO_2 from linear to bent. $CO_2^{\bullet-}$ is a highly unstable radical anion that almost immediately converts to CO_3^{2-}, CO, and $C_2O_4^{2-}$ [46]. If the transfer of the single electron occurs simultaneously with a proton transfer, the CO_2 reduction potential can be significantly lowered (i.e., more positive) due to the stabilization of $CO_2^{\bullet-}$ by the proton [37]. The reduction potential can be further reduced to a more positive value when multiple electrons and holes are simultaneously transferred to CO_2. Therefore, the multiple electron reduction of CO_2 is considered more thermodynamically favorable. Here, CO_2 typically converts to CO, CH_2O_2, CH_2O, CH_3OH, and CH_4. Although more thermodynamically favorable, these multiple electron reactions are kinetically more challenging and lead to difficulties in process efficiency and selectivity.

As depicted in Figure 3, any photocatalytic reaction mechanism generally involves the following steps [47]; (1) reactant adsorption onto active sites, (2) light absorption from the catalyst with subsequent photogeneration of e^- and h^+, (3) interaction between charges and adsorbed reactants, (4) redox reactions, and (5) product desorption. Nonetheless, the particular reaction mechanism of CO_2 photocatalysis is fairly complex. The reduction process, which is significantly influenced by the type of photocatalyst used, can give rise to a range of various possible products. The mechanism is also highly dependent on the energy of the photoexcited charges. If the excited charge carriers do not have the sufficient energy to react with the intermediate species, the reaction will not proceed and the final expected product from the photocatalytic reaction pathway will not be formed. Other factors that may inhibit the formation of products include product accumulation on the photocatalytic surface and photocatalyst deactivation. Moreover, the formed products might re-oxidize back to CO_2 in oxygen-rich environments. As a result of the aforementioned challenges, the yield of CO_2 photoreduction is usually very low and, as such, the formed products are generally difficult to detect [39].

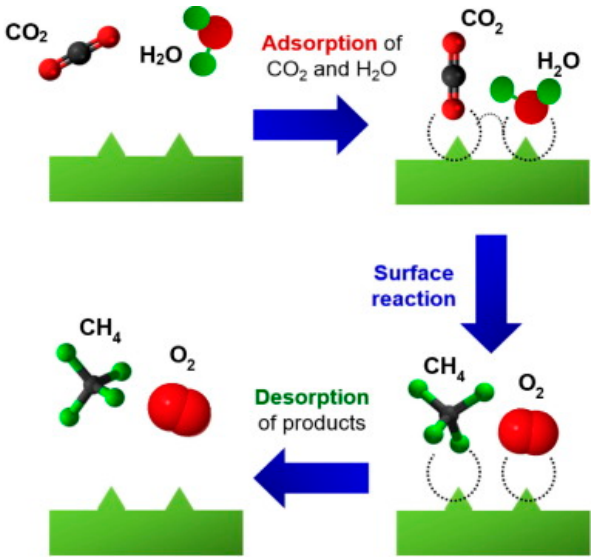

Figure 3. Basic illustration describing the reaction mechanism of CO_2 photoreduction. Reproduced from work in [47]. Copyright 2016 Elsevier B.V.

The kinetic modeling of CO_2 photoreduction has only been investigated by few. In these studies, two insights have been suggested on the rate limiting step. The first proposition claims that the activation of CO_2 through charge transfer is rate limiting [48]. In their mechanistic study, Uner et al. [49] suggested that the rate of the overall process of CO_2 photoreduction was limited by the production of electrons and protons. The second proposition claims that the reactant adsorption/product desorption is rate limiting [48]. A kinetic model proposed by Saladin et al. [50] demonstrated that product desorption was rate limiting at low temperatures while reactant adsorption was rate limiting at high temperatures. Further studies need to be conducted to help advance the understanding of reaction kinetics in CO_2 photoreduction.

Due to its availability and low cost, water is a desirable reducing agent to provide hydrogen atoms in the photocatalytic conversion of CO_2. It reacts with holes (h^+) to form O_2 and H^+. The H^+ ions later interact with the excited electrons (e^-) producing H_2 [51]:

$$2H_2O + 4h^+ \rightarrow O_2 + 4H^+ \qquad E = 0.81\ V, \tag{2}$$

$$2H^+ + 2e^- \rightarrow H_2 \qquad E = -0.42\ V, \tag{3}$$

Together, the CO_2 and the H^+ react and lead to the formation of stable molecules as shown in the equations below [51].

$$CO_2 + 2H^+ + 2e^- \rightarrow CO + H_2O \qquad E = -0.53\ V, \tag{4}$$

$$CO_2 + 2H^+ + 2e^- \rightarrow HCOOH \qquad E = -0.61\ V, \tag{5}$$

$$CO_2 + 4H^+ + 4e^- \rightarrow HCHO + H_2O \qquad E = -0.48\ V, \tag{6}$$

$$CO_2 + 6H^+ + 6e^- \rightarrow CH_3OH + H_2O \qquad E = -0.38\ V, \tag{7}$$

$$CO_2 + 8H^+ + 8e^- \rightarrow CH_4 + 2H_2O \qquad E = -0.24\ V, \tag{8}$$

Studies have shown that the presence of water in the reaction system favors the formation of methane as the major CO_2 reduction product [37]. Two fundamental mechanisms have been proposed for this specific reaction. One mechanism suggests that methane is produced in series [52]:

$$CO_2 \rightarrow HCOOH \rightarrow HCHO \rightarrow CH_3OH \rightarrow CH_4, \tag{9}$$

The second mechanism assumes that methane forms in parallel with methanol [53]:

$$CO_2 \rightarrow CO \rightarrow CH_3OH/CH_4, \quad (10)$$

Evidently, the reaction pathway of CO_2 photoconversion also greatly depends on the phase (liquid/vapor) of water, which has to be considered as an important reaction parameter [39]. The major product of CO_2 photoreduction in aqueous media is usually formic acid (Figure 4), whereas the main product in gaseous phase is typically CO (Figure 5). It is important to note that although methanol and methane are the desired end products, the reaction usually does not proceed to that point. Instead, it typically stops after the formation of formic acid or CO.

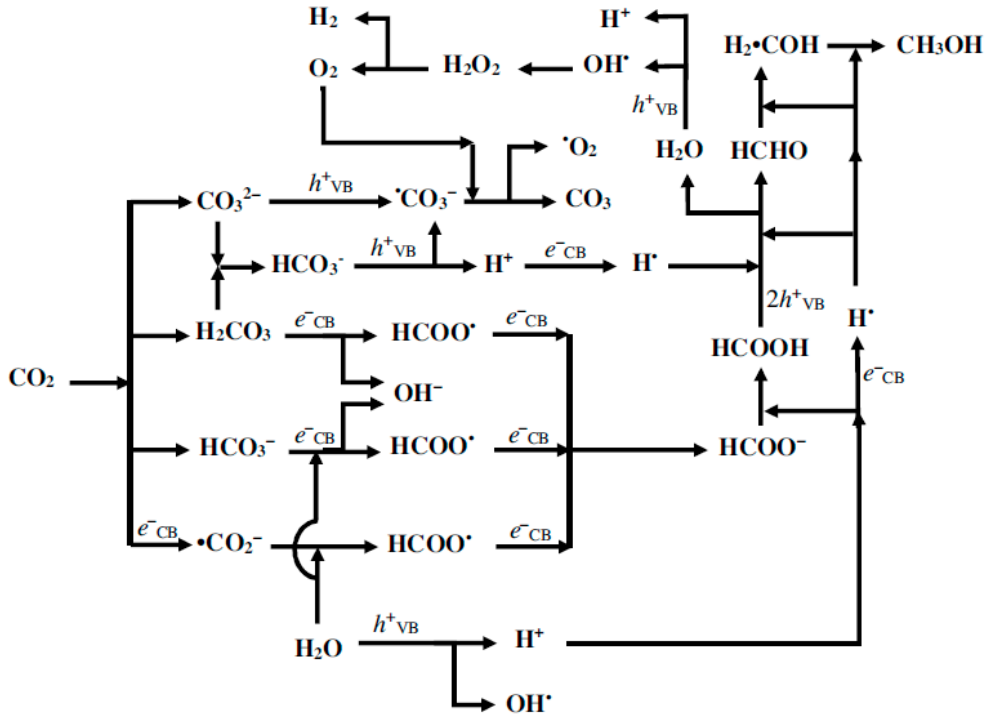

Figure 4. Aqueous phase photocatalysis of CO_2 and water: proposed reaction pathway. Reproduced from work in [39]. Copyright 2016 Elsevier Ltd.

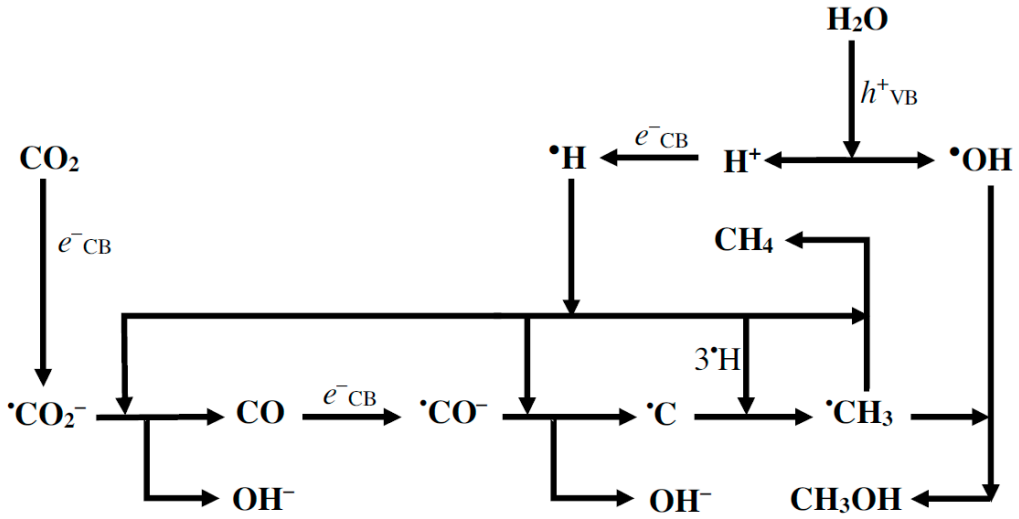

Figure 5. Gaseous phase photocatalysis of CO_2 and water: proposed reaction pathway. Reproduced from work in [39]. Copyright 2016 Elsevier Ltd.

Despite the aforementioned, the use of water has some limitations, including low CO_2 solubility (relevant when H_2O is used as the solvent), competing reduction reaction leading to hydrogen, and weak reducibility, eventually lowering the CO_2 conversion efficiency [38]. The photoreduction of water to hydrogen requires lower energy (E = 0 V) than the photoreduction of CO_2 (E = −1.90 V) and is, therefore, considered a strongly competing reduction process [39]. Furthermore, the photoreduction of CO_2 involves a multi-step charge transfer mechanistic approach in contrast to the single electron transfer step sufficient to initiate the photoreduction of water to hydrogen [37]. Due to these thermodynamic and kinetic limitations, and depending on the reductant used to obtain hydrogen, the generation of hydrogen from water photoreduction might occur with efficiency much higher than that of CO_2 photoreduction. Thus, when water is used as a reductant in the photocatalytic conversion of CO_2, hydrogen can appear as the predominant product. In addition, the higher dipole moment of water (D = 1.85), when compared to that of CO_2 (D = 0), favors its adsorption on the surface of the photocatalyst leading to another competing process [54]. The adsorption equilibrium constants of CO_2 and water vapor were determined in a study performed by Tan et al. [47]. Results showed that water vapor had a considerably higher adsorption equilibrium constant (8.07 bar^{-1}) than that of CO_2 (0.019 bar^{-1}). This implies that CO_2 adsorbs weakly on the surface of the photocatalyst. Ideally, and as discussed earlier in this section, CO_2 adsorbs to a photocatalyst surface in a bent configuration, whereby the carbon atom of CO_2 binds to a surface oxygen site while the oxygen atom binds to the surface metal center. This, however, is only applicable in the absence of water. Molecular dynamics studies were employed by Klyukin et al. [55] to help investigate the surface adsorption of CO_2 in the presence of water. Simulations showed that CO_2 adsorbed at oxygen sites while water saturated the metal sites. To manage the competitive adsorption between CO_2 and water, an optimum concentration of both reactants must be carefully considered. If CO_2 was present at extremely high concentrations, then it would effectively compete with water for the reactive sites. On the other hand, at CO_2 concentrations lower than that of water, only a limited number of CO_2 molecules would adsorb on the photocatalyst surface [47]. The formation of water-soluble products that are difficult to recover is another challenge faced in presence of water [37].

To help overcome the drawbacks of water as a reducing agent, many researches are currently investigating the use of alternative reductants for the photocatalytic conversion of CO_2. In this respect, the dielectric constant (κ) of the reducing agent significantly impacts the conversions and yields of the photocatalytic process. Solvents with varying dielectric constants (κ), including water (78.5), acetonitrile (37.5), 2-propanol (18.3), and dichloromethane (9.1), were tested as reducing agents in the photocatalytic reduction of CO_2 [56]. As κ increased, the conversion to formate increased while that to carbon monoxide decreased. This may be explained by the stabilization of the $CO_2^{\bullet-}$ radical by solvents with higher κ. Consequently, the more stable anion radical will interact more weakly with the photocatalytic surface.

As methanol is a strong reducing agent and has high CO_2 solubility, Qin et al. [38] investigated its use as a reductant for the photoreduction of CO_2 on a CuO-TiO_2 composite catalyst. Results show that CO_2 was reduced to produce methyl formate with a yield of 1602 μmol/g-cat/h. In addition, other studies on the photocatalytic reduction of CO_2 in a solution of NaOH showed that the use of NaOH as a reductant enhances the photocatalytic efficiency [57,58]. In this respect, CO_2 absorbs chemically in NaOH solutions due to its acidic properties leading to a concentration much higher than in DI water, and moreover the OH^- present in solution may serve as strong hole scavenger, enhancing charge separation. The optimal concentration of NaOH was reported to be 0.2 M [57,58].

Studies have also shown that the conversion of CO_2 using hydrogen as a reducing agent is higher than that when water is used [59]. This is because the photoreduction of CO_2 with hydrogen is more thermodynamically favorable than that with water [39]. Lo et al. [60] studied the photocatalytic conversion of CO_2 using bare TiO_2 (Evonik P-25) under UV irradiation. Three different reductants were tested: water, hydrogen, and water + hydrogen. The results, which are presented in Figure 6, show that the highest product yields of CO_2 photoreduction were obtained when hydrogen and saturated

water vapor were used together as reductants, producing methane, carbon monoxide and ethane with a yield of 4.11, 0.14, and 0.10 μmol/g-cat/h, respectively. The authors propose that water accelerated the photoreduction of CO_2 with hydrogen by donating electrons and subsequently inhibiting charge recombination. They also suggest that water supplied more hydrogen atoms for the photoreduction of CO_2.

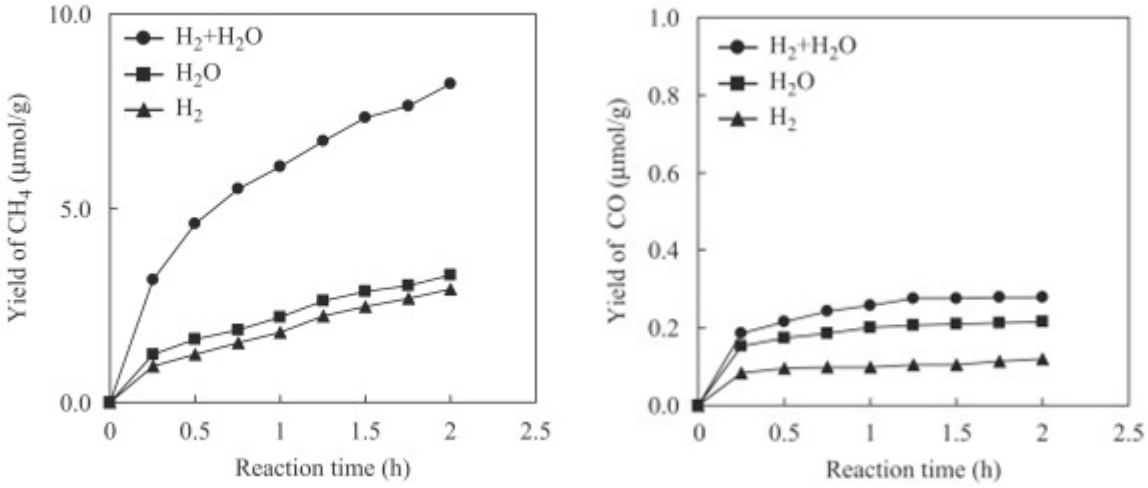

Figure 6. Effect of reductant on the yield of CO_2 photoreduction products, i.e., CH_4 (**a**) and CO (**b**). Reproduced from work in [60]. Copyright 2007 Elsevier B.V.

The photocatalytic reduction of compressed CO_2 (either liquid or supercritical) might be considered as an alternative solution to the use of organic solvents, but it has been rarely investigated [61]. Kaneco et al. [62] performed a study on the photoreduction of liquefied CO_2 using TiO_2 as the catalyst and water as the reducing agent. Results show the highly selective formation of formic acid with no other reduction products detected. Kaneco et al. [63] also investigated the photocatalytic reduction of CO_2 into formic acid in supercritical CO_2. The photoreduction reaction was conducted at 9.0 MPa and 35 °C with TiO_2 as the catalyst. Under these conditions, the production rate of formic acid reached a maximum yield of 1.76 μmol/g-cat/h. Kometani et al. [64] examined the photocatalytic reduction of CO_2 in a supercritical mixture of water and carbon dioxide (400 °C and 30 MPa) using Pt–TiO_2 as the catalyst. Carbon monoxide, methane, formic acid, and formaldehyde were all detected as reaction products with yields much higher than those obtained from the same reaction but at room temperature. Despite the enhanced product yields, the major drawback in using compressed CO_2 is the large amount of energy required to change its state from gas to liquid or to supercritical. One possible suggestion to help mitigate this limitation could be to target industrial processes that already utilize CO_2 in its compressed form. Thus, the overall energy efficiency of the photoreduction process could be greatly enhanced.

3. Titanium Dioxide: Synthesis and Surface Modification Strategies for Enhanced CO_2 Photoreduction

As shown in Figure 7, TiO_2 exists as one of three mineral phases: anatase, brookite, and rutile. Anatase-phase TiO_2 is the most common phase of TiO_2, but has a band gap of 3.2 eV, and is therefore weakly active under visible light. Rutile-phase, with a band gap of 3.0 eV, has the strongest visible light absorption, whereas brookite (band gap = 3.3 eV) has the weakest [65]. The use of mixed-phase TiO_2 enhances both the visible light harvesting ability and the electron–hole separation of TiO_2 [66]. The crystalline phase of TiO_2 is highly dependent on its preparation technique.

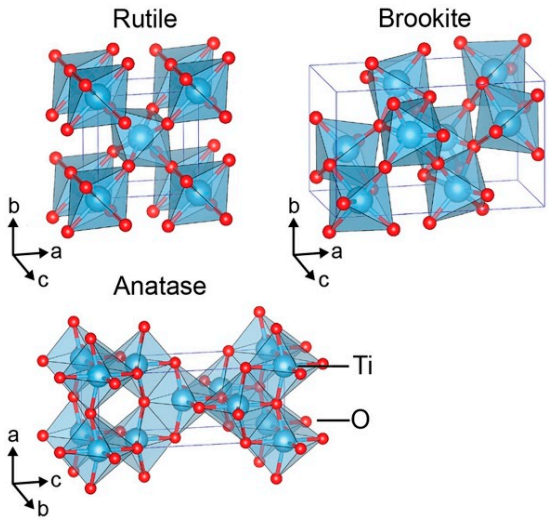

Figure 7. Crystal structures of TiO_2. Reproduced from work in [67].

The sol–gel method is widely used among researches for the preparation of bare and doped TiO_2-based photocatalysts both as thin films or powders [68]. This is attributed to the many benefits of this simple and cost effective method, which include the synthesis of nano-sized crystallized powder of high purity and homogeneity at relatively low temperature, possibility of tuning stoichiometry and morphology and easy preparation of composite materials [69,70]. Other photocatalysts such as ZrO_2 [71], ZnO [72], and WO_3 [73] have also been fabricated via the sol–gel process.

In general, the one-pot sol–gel procedure, shown in Figure 8, consists of two processes: hydrolysis and condensation. During these processes, the metallic atoms of the precursor molecules bind to form metal oxides and metal hydroxides. In the case of TiO_2, titanium alkoxides, such as titanium isopropoxide or titanium n-butoxide, are used as the precursor. Alcohol and acid must also be introduced into the reaction system as reaction modifiers. A densely cross-linked 3D TiO_2 gel with large specific surface area is formed as an end product after allowing the mixture of precursor, alcohol and acid to stir for several hours [70]. The choice of reaction parameters including reactants molar ratio, solution pH, reaction temperature, and reaction time, significantly affect the morphology of the final catalyst [74,75]. For instance, different reactant molar ratios would result in different hydrolysis rates which would in turn return structurally different TiO_2 catalysts [76,77]. Another example is the choice of acid where using acetic acid in the sol–gel synthesis of TiO_2 was shown to favor the formation of anatase-phase TiO_2, whereas using hydrochloric acid favored the formation of brookite and rutile mixed-phase TiO_2. Post-synthesis treatment techniques such as aging, drying and annealing are sometimes utilized to enhance the activity of the synthesized TiO_2 photocatalyst [78]. To develop TiO_2 films, the viscous sol may be deposited on a substrate via film coating techniques [79,80].

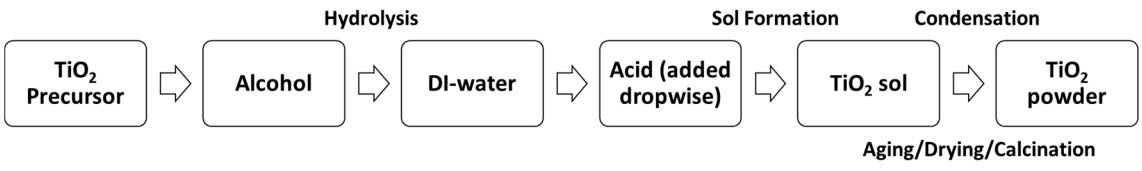

Figure 8. Sol–gel method for the preparation of bare and doped TiO_2-based photocatalysts.

The hydro/solvo thermal method is another one-pot TiO_2 synthesis technique that takes place in an aqueous solution above room temperature and atmospheric pressure [81]. More specifically, the TiO_2 precursor (titanium alkoxides) is mixed with an aqueous solution of an acid or a base for 16 to 72 h at high reaction temperature (110–180 °C). Post-synthesis treatment, which includes washing

the obtained precipitate with DI water and then dispersing it in HCl solution before calcination, is usually performed to enhance the nanostructure of TiO_2. Quenching, or rapid cooling, is also commonly applied post-synthesis to enhance the photocatalytic activity of TiO_2 [82]. The hydro/solvo thermal process yields highly pure and well-defined TiO_2 nanocrystals with narrow particle size distribution [70]. Depending on the synthesis process parameters, which include the choice of precursor, the concentration of acidic/alkaline solution and the reaction temperature and time, different TiO_2 morphologies may be obtained. This ability to control the synthesis process to obtain TiO_2 as nanoparticles, nanotubes, nanoribbons, or nanowires is a great advantage of the hydro/solvo thermal treatment technique [83–85].

A number of studies have reported the significant CO_2 photocatalytic conversion improvement of TiO_2-based catalysts when synthesized under supercritical conditions. Camarillo et al. [86] prepared TiO_2 catalysts in supercritical CO_2 via a hydrothermal method. The synthesized TiO_2 catalyst was used for the photoreduction of CO_2 to methane, where the catalyst exhibited better photoactivity than the standard reference catalyst Evonik P-25. When prepared in supercritical CO_2, TiO_2 displayed improved CO_2 adsorption, enhanced charge separation and stronger visible light absorption. The highest methane production rate of 1.13 μmol/g-cat/h was obtained when diisopropoxititanium bis(acetylacetonate) precursor and isopropyl alcohol were used in the catalyst preparation.

The choice of precursor significantly affects the photocatalytic property of the synthesized catalyst. Bellardita et al. [87] prepared TiO_2 photocatalysts via the hydrothermal method using two different precursors, titanium tetrachloride and titanium butoxide. The TiO_2 photocatalysts were tested for the reduction of CO_2 and results showed that the photocatalysts synthesized from titanium tetrachloride favored the formation of formaldehyde, whereas those synthesized from titanium butoxide favored the formation of methane. The same study also examined the use of copper-doped TiO_2 for the photoreduction of CO_2. Results showed that doping TiO_2, synthesized with titanium tetrachloride precursor, with 1 wt.% copper enhanced the formaldehyde production rate. However, doping TiO_2, synthesized with titanium butoxide precursor, with 1 wt.% copper decreased the methane production rate.

The catalyst morphology plays a crucial role in determining its photocatalytic efficiency. TiO_2 nanostructures (nanosheets, nanorods, nanowires, nanotubes, nanobelts, etc.) have been shown to exhibit superior performance for photocatalytic reduction of CO_2 [26]. These nanostructures provide large surface area, reduced grain boundaries, and facile charge transport paths. Specifically, reduced grain boundaries and defects usually lead to a direct pathway for electron transport to catalytic sites, inhibiting the electron–hole recombination rate.

The use of unmodified TiO_2 photocatalysts for the reduction of CO_2 under UV light has been reported by many to be inefficient [37]. This is mainly attributed to the reduction potential (−0.5 V) of electrons in the TiO_2 CB which is much lower (i.e., more positive) than the theoretical thermodynamic requirement for the single electron reduction of CO_2 (−1.90 V). To drive any reduction process, the potential of the CB must be more negative than that of the reduction reaction [39]. This is true in the case of the multiple electron reduction of CO_2 to methane (−0.24 V) or to methanol (−0.38 V). On the other hand, the co-presence of strong reducing electrons and free protons is detrimental as they may interact to produce molecular hydrogen. This may be avoided by introducing spatially separated centers within the TiO_2 lattice in order to trap the charges and reduce their recombination [37].

Several modification strategies have been suggested to help overcome the drawbacks of TiO_2. Many of these strategies are shown in Figure 9 and they include metal deposition, metal/non-metal doping, loading of carbon-based material, formation of semiconductor heterostructures, and dispersion on high surface area supports. All of the aforementioned techniques serve to enhance the separation of electrons and holes and to extend the absorption of light into the visible range. Loading TiO_2 with carbon-based materials and dispersing TiO_2 on inert supports offers the added advantages of increasing the concentration of surface electrons, improving the surface adsorption of reactants (specifically CO_2), and reducing the agglomeration of TiO_2 nanoparticles. Nonetheless, the utilization

of carbon-based materials hinders the absorption of light while high surface area supports lower the light utilization efficiency since they absorb and scatter part of the radiation resulting in a waste of photons. Although TiO_2-based heterostructures are complex to synthesize and are considered to be relatively unstable, they effectively separate oxidation and reduction sites improving the photocatalytic performance of TiO_2 semiconductors. To overcome limitations and drawbacks, many researches have suggested to employ hybrid systems which combine two or more of these different modification techniques [40]. The advantages and disadvantages of the main modification strategies along with the performance results from the most important CO_2 photoreduction studies are summarized in Tables 1 and 2 below [19,26,37,88–90]. Further details on the pros and cons of the mentioned TiO_2 surface modification techniques are discussed in the following individual Sections 3.1–3.5

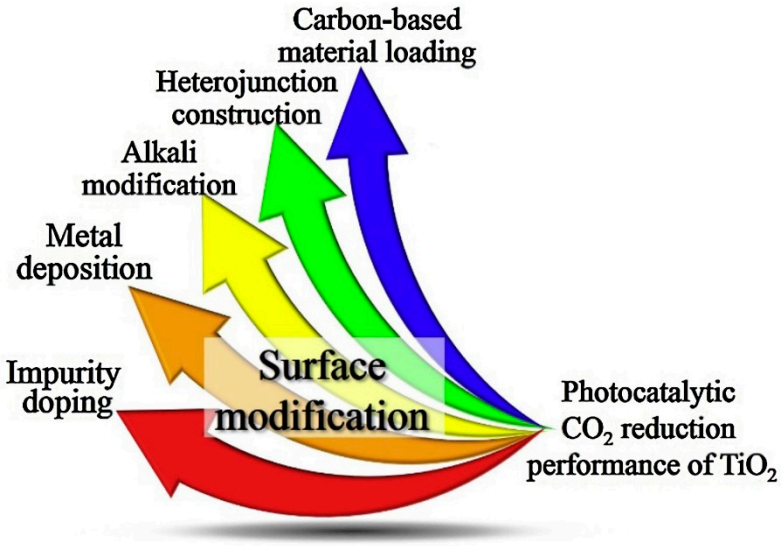

Figure 9. Photocatalyst modification strategies. Reproduced from work in [40]. Copyright 2016 Elsevier B.V.

Table 1. Advantages and disadvantages of TiO_2 modification techniques.

Modification Strategy	Advantages	Disadvantages
Metal Deposition	-Enhances electron–hole separation	-Expensive -Rare
Metal Doping	-Extends light absorption into visible range -Enhances electron–hole separation	-Act as recombination centers -Leads to structural defects -Possibility of metal leaching
Non-Metal Doping	-Extends light absorption into visible range -Enhances electron–hole separation	-Act as recombination centers
Carbon-based Material Loading	-Extends light absorption into visible range -Enhances electron–hole separation -Increases electron concentration on TiO_2 surface -Improves CO_2 adsorption on catalytic surface -Reduces agglomeration of TiO_2 nanoparticles	-Forbids light absorption by TiO_2
Heterostructures	-Extends light absorption into visible range -Enhances electron–hole separation -Separates reduction and oxidation sites	-Complex synthesis method -Instability
Dispersion on Supports	-Enhances the catalyst's product selectivity, pore structure and electronic properties -Eliminates need for post treatment separation -Provides high surface area -Enhances dispersion of TiO_2 nanoparticles	-Low light utilization efficiency
Alkali Modification	-Improves adsorption of reactants on catalytic surface -Enhances electron–hole separation -Enhances the chemisorption of CO_2	-Encapsulation of TiO_2 nanoparticles

Table 2. Photocatalytic performance of various TiO_2-based catalysts in the reduction of CO_2*.

Modification Strategy	Photocatalyst	Synthesis Method	Reductant	Light Source	Main Product Yield (μmol/g-cat/h)	Ref.
Metal Deposition *Platinum*	One-dimensional TiO_2 single crystals coated with ultrafine Pt NPs	CVD	Water	UV	Methane: 1361	[91]
	0.2 wt.% Pt on mesoporous TiO_2	Soft Template	Water	UV	Methane: 2.85	[36]
Metal Deposition *Gold*	0.5 wt.% Au on TiO_2 NWs	HT	Hydrogen	Visible	Carbon monoxide: 1237 Methanol: 12.65	[92]
Metal Deposition *Silver*	Ag-electrodeposited on TiO_2 NRs	HT	Water	UV	Methane: 2.64	[93]
Metal Deposition *Copper*	1.7 wt.% Cu and 0.9 wt.% Pt NPs on TiO_2 (Evonik P-25)	-	Water	UV + Visible	Methane: 33	[94]
	Cu/C–TiO_2	Sol–gel	Water	UV	Methane: 2.526	[95]
Metal Doping *Copper*	1.2 wt.% Cu-TiO_2	HT	Water	UV	Methanol: 0.45	[96]
	2 wt.% Cu-TiO_2	Sol–gel	NaOH	UV	Methanol: 12.5	[58]
	3 wt.% Cu-TiO_2 (Evonik P-25)	-	$KHCO_3$	UV	Methanol: 194	[97]
Metal Doping *Nickel*	0.1 mol % Ni-TiO_2	ST	Water	UV	Methane: 14	[98]
Metal Doping *Cerium*	0.28 mol % Ce-TiO_2	Sol–gel	NaOH	UV	Methane: 0.889	[99]
Non-Metal Doping *Nitrogen*	N-TiO_2 NTs	HT	NaOH	Visible	Formic acid: 1039 Methanol: 94.4 Formaldehyde: 76.8	[100]
Non-Metal Doping *Carbon*	C–TiO_2	IMM	Na_2SO_3	Solar	Formic acid: 439	[101]
Carbon-based Material Loading *CNTs*	MWCNT/TiO_2 nanocomposite	-	Water	Visible	Methane: 0.17	[102]
	Anatase-TiO_2 NPs/MWCNT	Sol–gel	Water	UV	Ethanol: 29.872	[103]
	Rutile-TiO_2 NRs/MWCNT	HT	Water	UV	Formic acid: 25.02	[103]
	CNT-Ni/TiO_2 nanocomposites	CVD	Water	Visible	Methane: 0.145	[104]
Carbon-based Material Loading *Graphene*	Graphene/ N-TiO_2	ST	Water	Visible	Methane: 0.37	[105]
Hetero-structures	1 wt.% CuO-TiO_2 composite	-	Methanol	UV	Methyl formate: 1602	[38]
Dispersion on Supports	0.5 wt.% Cu/TiO_2-silica nanocomposite	Sol–gel	Water	UV	Carbon monoxide: 60 Methane: 10	[106]
Alkali Modification	3 wt.% NaOH-TiO_2	IMP	Water	UV	Methane: 8.667	[90]

* Abbreviations: NP: nanoparticle; NW: nanowire; NR: nanorod; NT: nanotube; CVD: chemical vapor deposition; HT: hydrothermal; ST: solvothermal; IMM: immersion; IMP: impregnation; MWCNT: multiwall carbon nanotubes; UV: ultraviolet.

3.1. Metal Deposition

Although considered an expensive modification technique, metal deposition enhances the electron–hole separation in a semiconductor, improving the photoreduction efficiency of CO_2 [40,107]. As the work function of the metal increases, the metal's ability to accept the photogenerated electrons also increases [36,40]. This in turn enhances the electron–hole separation and the overall photocatalytic activity of TiO_2. Some of the most commonly deposited metals arranged in order of highest work function include platinum (5.93 eV), palladium (5.60 eV), gold (5.47 eV), and silver (4.74 eV) [25,40].

Wang et al. [91] demonstrated high CO_2 photoreduction efficiency of one-dimensional (1D) TiO_2 single crystals coated with ultrafine Pt nanoparticles. This efficient Pt–TiO_2 nanofilm, shown in Figure 10, was synthesized via chemical vapor deposition and exhibited selective formation of methane with a maximum yield of 1361 μmol/g-cat/h. Deposition of Pt nanoparticles enhanced the electron–hole separation leading to a more efficient photocatalytic performance. Li et al. [36] also proposed the use of Pt-deposited TiO_2 for the photoreduction of CO_2 to methane. Results showed that depositing 0.2 wt.% Pt on mesoporous TiO_2 yields methane with a production rate of 2.85 μmol/g-cat/h. Tostón et al. [108]

examined the photocatalytic activity of 1 wt.% Pt–TiO_2 photocatalysts prepared in supercritical CO_2. The synthesized photocatalyst was used to reduce CO_2 into methane. The study indicated that the use of supercritical CO_2 results in a photocatalyst with higher surface area, crystallization degree, pore volume, visible light absorbance, and methane production rate (0.245 μmol/g-cat/h).

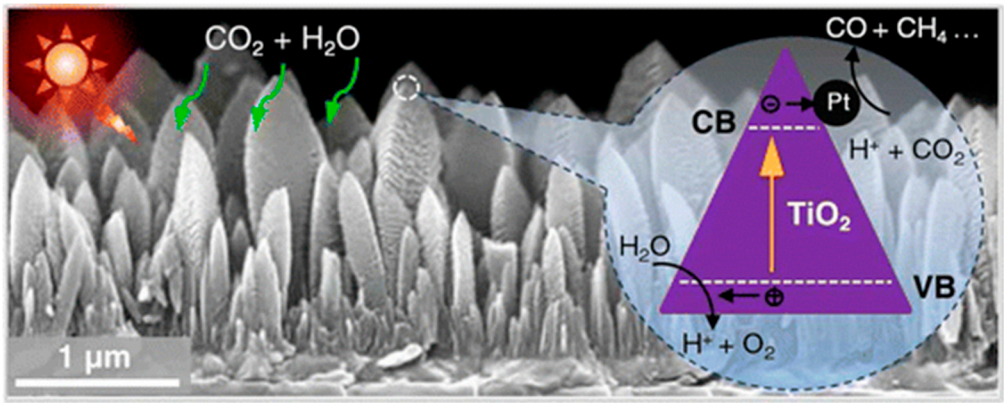

Figure 10. Enhanced CO_2 photoreduction efficiency by ultrafine Pt nanoparticles deposited on TiO_2 crystals. Reproduced from work in [91]. Copyright 2012 American Chemical Society.

Owing to the effect of localized surface plasmon resonance (LSPR) and to that of Schottky barrier formation, Au and Ag nanoparticles have been shown to enhance the visible-light activity of several semiconducting materials. In LSPR, an electromagnetic field is created and the photoreaction is improved via photon scattering, plasmon resonance energy transfer and hot electron excitation. On the other hand, the formation of a Schottky barrier enhances the photoactivity by trapping and prolonging the electron life [109]. Tahir et al. [92] described the photoreduction of CO_2 using Au-decorated TiO_2 nanowires, prepared by hydrothermal method. Deposition of 0.5 wt.% Au on the TiO_2 nanowires yielded 1237 μmol carbon monoxide/g-cat/h and 12.65 μmol methanol/g-cat/h. Surface deposition of Au nanoparticles enhanced charge separation and improved photocatalytic activity under visible light through plasmon excitation. More specifically, the LSPR effect of Au nanoparticles promotes electrons to the CB of TiO_2. The positively charged plasmas of Au nanoparticles then trap photogenerated CB electrons enhancing the separation of charges. Next, the LSPR effect of Au improves the energy of these trapped electrons and, as a result, the efficiency of CO_2 photoreduction increases [109]. Kong et al. [93] proposed the use of Ag-electrodeposited TiO_2 nanorods, prepared by hydrothermal method, for the photocatalytic reduction of CO_2 to methane. The photocatalyst exhibited enhanced photoactivity with a methane yield of 2.64 μmol/g-cat/h. This improved performance was attributed to the plasmonic characteristics of the Ag nanoparticles.

Murakami et al. [110] photocatalytically reduced CO_2 using Ag/Au-TiO_2. The deposited metal nanoparticles act as reductive sites increasing the production of methanol compared to that of bare TiO_2. Zhai et al. [94] photodeposited Cu and Pt nanoparticles on TiO_2 (Evonik P-25) using copper sulfate and chloroplatinic acid, respectively, as the metal precursors. Results showed the photo-depositing TiO_2 with 1.7 wt.% Cu and 0.9 wt.% Pt allowed to produce methane from CO_2 with a yield of 33 μmol/g-cat/h. Yan et al. [95] used a sol–gel method to synthesize a novel Cu/C–TiO_2 catalyst for the photoreduction of CO_2 in water under UV irradiation. Co-deposition of Cu and C onto the TiO_2 surface extended the light absorption into the visible range, reduced the electron–hole recombination rate and provided an increased number of reaction sites on the photocatalytic surface. The enhanced Cu/C–TiO_2 photocatalyst reduced CO_2 to methane with a production rate of 2.53 μmol/g-cat/h.

3.2. Doping

One of the many strategies used to enhance the activity of TiO_2 photocatalysts is doping with metals such as copper, nickel, silver and cerium. This technique is the most widely applied method used to extend the light absorption range and suppress the recombination rate of TiO_2. Although introducing metal nanoparticles into the TiO_2 matrix leads to structural defects, their presence reduces the TiO_2 bandgap, shifting the absorption threshold to visible [40]. The reduction in bandgap occurs as a consequence of the new energy level produced by the dispersion of dopants in the TiO_2 lattice [111]. Not only that, but the doped metal may also act as an electron trap, enhancing the separation of the photogenerated electrons and holes during irradiation as illustrated in Figure 11. One major drawback of metal doping is the possibility of metal leaching and, consequently, catalyst deactivation. This might occur as a result of the photocorrosion of doped TiO_2, especially when water is used as a reductant [37].

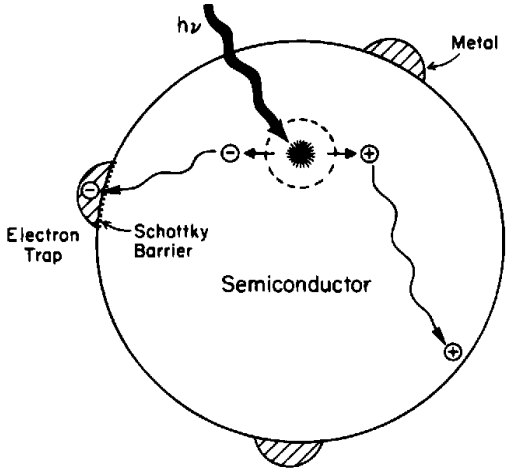

Figure 11. Electron–hole separation of metal-doped semiconductors. Reproduced from work in [112]. Copyright 1995 American Chemical Society.

To prepare metal-doped TiO_2, the sol–gel method is commonly followed due to its versatility and simplicity. In a typical process, a TiO_2 precursor is mixed with a metal-dopant precursor which has been dissolved in alcohol. After hydrolysis for several hours and at elevated temperatures, the reaction mixture is dried and a metal-doped catalyst in powder form is obtained [111]. Chemical vapor deposition and hydro/solvo-thermal techniques may also be used for the synthesis of metal-doped TiO_2.

One of the most commonly used metal dopants incorporated into TiO_2 semiconductors is copper. Different metal loading levels of Cu-doped TiO_2 were tested for the photocatalytic reduction of CO_2 under UV light. For instance, Wu et al. [96] reduced CO_2 to methanol using a Cu-doped TiO_2 catalyst under UV irradiation. The catalyst was synthesized via a hydrothermal method and exhibited a band gap of 3.3 eV. Doping TiO_2 with 1.2 wt.% copper produced methanol with a yield of 0.45 μmol/g-cat/h. Tseng et al. [58] reported the photocatalytic reduction of CO_2 into methanol under UV irradiation using copper-doped TiO_2, prepared using the sol–gel method. The results of this study showed that doping the TiO_2 catalyst with 2 wt.% copper gave the highest methanol yield of 12.5 μmol/g-cat/h. The copper doping lowered the electron–hole recombination probability, which consequently boosted the photocatalytic efficiency. Nasution et al. [97] studied the use of Cu-doped TiO_2 (Evonik P-25), prepared by an impregnation method, for the photocatalytic reduction of CO_2 under UV irradiation. Results showed that doping TiO_2 with 3 wt.% copper yields a maximum methanol production rate of 194 μmol/g-cat/h. All of the aforementioned studies suggest that the photocatalytic reduction of CO_2 using a Cu-doped TiO_2 catalyst under UV illumination yields methanol as the main reaction product.

Due to the LSPR effect of copper nanoparticles, Cu-doped TiO_2 has been shown to exhibit enhanced photocatalytic activity under visible light. The strong local electron field from the LSPR effect improves the energy of the trapped electrons resulting in an enhanced photocatalytic CO_2 reduction process. The concentration of copper dopant, however, must be carefully considered. Although excess copper nanoparticles improve the separation of charges, they also lead to the formation of larger copper particles. These larger particles have a weaker LSPR effect and as such considerably lower the photocatalytic efficiency [113].

The metal dopant concentration significantly affects the photocatalytic activity of doped TiO_2. Depending on its concentration, the metal dopant can either hinder or promote the anatase-to-rutile transformation during calcination. The crystal structure transformation to rutile reduces the catalyst's surface area and removes any active species present on the anatase surface, thereby lowering the catalytic performance of doped TiO_2 [114]. To maintain high anatase levels and therefore better photocatalytic activity, low concentrations of metals (0.1–0.5 mol %) are commonly doped into TiO_2. In addition to the structural transformation, the dopant loading level also influences the recombination of photogenerated charges. By acting as recombination centers, metal dopants, can significantly increase the electron–hole recombination especially when present at high concentrations (>3 mol %), therefore lowering the photocatalytic efficiency [115]. Kwak et al. [98] investigated the photocatalytic reduction of CO_2 to methane using a nickel-doped TiO_2 catalyst, prepared via a solvothermal method. Doping with 0.1 mol % nickel gave the highest methane yield of 14 μmol/g-cat/h. Matějová et al. [99] examined the photoactivity of cerium-doped TiO_2, synthesized by the sol–gel method, for the reduction of CO_2. The doped cerium shifted the light absorption of the catalyst into the visible range and enhanced charge separation. Results showed that doping TiO_2 with 0.28 mol % cerium gave the highest methane yield of 0.889 μmol/g-cat/h.

Nonmetal dopants, such as nitrogen, carbon, sulfur, and fluoride, are commonly used to help reduce the TiO_2 band gap, consequently increasing the absorption of visible light [26]. Substitutional nonmetal doping typically introduces defect states localized at the impurity site which reduce the band gap and induce absorption in the visible region. Furthermore, these defect states, which form below the conduction band, have been shown to be good acceptors of electrons. Nonetheless, nonmetal doping also leads to the formation of oxygen vacancies. These oxygen vacancy defects generally act as charge recombination centers which are detrimental in photocatalytic reactions and must therefore be avoided [116]. As the quantity of nonmetal dopant increases, the amount of defects increases and the photocatalytic activity consequently decreases. Therefore, in nonmetal doping, extra care must be taken in optimizing the dopant concentration for enhanced visible light absorption and improved photocatalytic activity with an acceptable extent of defects [117]. One strategy commonly used to reduce the recombination of charges in nonmetal doped TiO_2 is co-doping with an electron donor–acceptor pair [118]. Similar to metal-doping, non-metal doping is usually performed via the sol–gel process, although other techniques including hydro/solvo-thermal methods may also be applied.

Studies have shown that the main reaction product resulting from the photocatalytic conversion of CO_2 using non-metal dopants is formic acid. For example, Zhao et al. [100] studied the photocatalytic activity of nitrogen-doped TiO_2 nanotubes prepared by a hydrothermal method, where titanium (III) chloride and hexamethylene tetramine were used as precursors. As a doping agent, nitrogen extended the light absorption of TiO_2 into the visible range. The formic acid yield was 1039 μmol/g-cat/h, the methanol yield was 94.4 μmol/g-cat/h, and the formaldehyde yield was 76.8 μmol/g-cat/h. Xue et al. [101] investigated the non-metal, substitutional doping of TiO_2 with carbon using citric acid as a precursor. The doped carbon lowered the TiO_2 band gap, shifting the light absorption into the visible range, and improved the charge separation efficiency. CO_2 was photocatalytically reduced to yield 439 μmol formic acid/g-cat/h.

3.3. Carbon-Based Material Loading

The incorporation of carbon-based materials into TiO_2 catalysts is gaining wide interest in the field of photocatalysis. This is mainly due to the carbon-based materials' properties such as their abundancy, low cost, good corrosion resistance, high electron conductivity, large specific surface area, and tunable surface properties. Although in most cases they reduce the light absorbed by TiO_2, loading the catalyst with carbon based-materials, such as carbon nanotubes or graphene, enhances the electron–hole separation, the electron concentration on the TiO_2 surface, and the CO_2 adsorption through π–π conjugations between CO_2 molecules and the carbon-based material [40].

Carbon nanotubes are regarded to be among the most remarkable emerging materials mainly due to their unique electronic, adsorption, mechanical, chemical, and thermal characteristics [119]. Advances in the synthesis techniques of multiwalled carbon nanotubes (MWCNTs) have resulted in a significant reduction of the material's cost, consequently allowing for their use on a large industrial scale [103]. In addition to that, the mesoporosity of carbon nanotubes, which favors the diffusion of reacting species, is an added value of this widely investigated material [120]. Many recent studies have focused on developing synthesis methods to combine carbon nanotubes with semiconducting catalysts, such as TiO_2. This new hybrid composite is believed to enhance the efficiency of many photocatalytic applications, especially with its improved charge transfer properties and the formation of new active sites [103,120]. The main disadvantage in synthesizing MWCNT/TiO_2 hybrids is the need for treating the carbon nanotubes with strong acids in order to introduce the functional groups to the surface [120]. A range of different techniques has been employed for the fabrication of MWCNT/TiO_2 composites: mechanical mixing [121], sol–gel [122], electrospinning [123,124], and chemical vapor deposition [125]. Depending on the choice of the synthetic strategy, composite materials with different coating uniformity and varying physical characteristics are prepared. More specifically, uniform TiO_2 coatings on carbon nanotubes may be achieved through electrospinning and chemical vapor deposition, whereas other methods such as sol–gel typically yield nonuniform coatings with TiO_2 aggregates being randomly dispersed on the carbon nanotube surface [126]. On the other hand, chemical vapor deposition and electrospinning are complex techniques which require the use of specialized equipment.

Using the process shown in Figure 12, Gui et al. [102] prepared a MWCNT/TiO_2 nanocomposite for the photocatalytic reduction of CO_2. The MWCNTs enhanced the TiO_2 photoactivity under visible light, yielding 0.17 μmol methane/g-catalyst/h. Xia et al. [103] studied the effect of using two different methods of synthesis—sol–gel and hydrothermal—for the preparation of MWCNT-supported TiO_2 composite. The sol–gel method formed anatase-phase TiO_2 nanoparticles on the MWCNT, whereas rutile-phase TiO_2 nanorods were formed when the hydrothermal method was used. In addition to that, the MWCNT/TiO_2 composite prepared via sol–gel mainly reduced CO_2 to ethanol (29.87 μmol/g-cat/h), whereas the composite prepared hydrothermally mainly reduced CO_2 to formic acid (25.02 μmol/g-cat/h). The efficiency of the CO_2 photoreduction reaction was significantly enhanced with the incorporation of MWCNTs. More specifically, the MWCNTs helped reduce the agglomeration of TiO_2 nanoparticles and helped increase the separation of the photogenerated electron–hole pairs. Ong et al. [104] demonstrated the photocatalytic activity of CNT-Ni/TiO_2 nanocomposites in reducing CO_2 to methane under visible light. The nanocomposite, prepared by chemical vapor deposition, exhibited a reduced band gap of 2.22 eV and a methane yield of 0.145 μmol/g-cat/h.

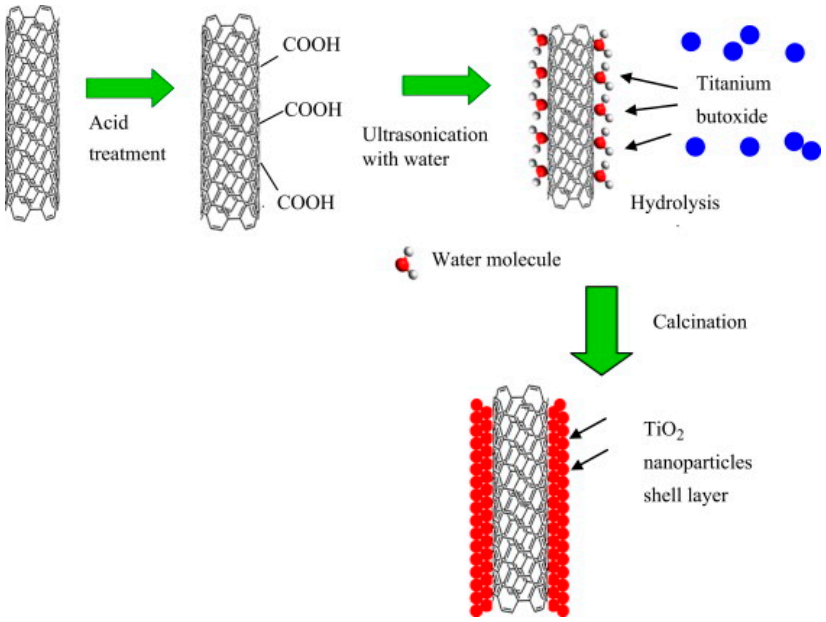

Figure 12. Enhanced visible light responsive MWCNT/TiO_2 core–shell nanocomposites for photocatalytic reduction of CO_2. Reproduced from work in [102]. Copyright 2013 Elsevier B.V.

Graphene is a 2-D, single layer of graphite with outstanding physiochemical properties including low production costs, ease of scalability, exceptional catalytic performance, high mechanical strength, high porosity, high thermal and electrical conductivity, remarkably high CO_2 adsorption capacity, high transparency, high flexibility, and high specific surface area. Furthermore, the exceptional photocatalytic properties of graphene, which include zero band gap, large BET area and high electron mobility, have encouraged its use in many photocatalytic applications [127]. Many different types of semiconducting photocatalysts have been coupled with graphene with the aim of enhancing the overall efficiency of photocatalysts [128,129]. The preparation process greatly affects the morphology, structure, size, properties, and activity of the composite photocatalyst [130]. The methods commonly used for the preparation of graphene-based TiO_2 are generally divided into two main categories: in situ crystallization (including hydrothermal/solvothermal, sol–gel, microwave assisted and others) and ex situ hybridization (including solution mixing, self-assembly, electrospinning and others). It is important to note that molecular linkers between TiO_2 and the graphene sheets are not required during the synthesis of the composite [131]. This is a great benefit since molecular linkers might act as electron traps decreasing the overall photocatalytic efficiency of the graphene-based TiO_2 composite.

In general, both the hydrothermal and the solvothermal processes are characterized by their high reactivity, low energy requirement, mild reaction conditions, relatively environmental set-up, and simple solvent control. Under optimal conditions, both techniques can yield large quantities of graphene-based photocatalysts at low cost [129]. Furthermore, TiO_2 nanostructures with high crystallinity are typically produced through the one-pot hydrothermal/solvothermal approach without the need for post-synthesis calcination [132]. Experimental conditions, including precursor concentration, pH, temperature, and time, significantly affect the reaction pathway and the nanomaterial's crystallinity and, therefore, must be carefully considered [129,132].

In sol–gel techniques and through a series of hydrolysis and condensation steps, a liquid colloidal solution "sol" containing graphene/graphene oxide and TiO_2 precursor is transitioned into a xerogel [129,132]. The hydroxyl groups present on the surface of the graphene oxide sheets provide nucleation sites for hydrolysis [129]. Consequently, the TiO_2 nanoparticles will be strongly bonded to graphene, offering a great advantage over other synthesis methods [133].

Solution mixing is fairly simple and involves only the mixing of a TiO_2 precursor in a suspension of graphene oxide under vigorous/ultrasonic agitation. Simple treatments, including drying and calcination, may be utilized after synthesis to improve the photocatalytic efficiency of the final composite material [130]. Furthermore, graphene oxide may be reduced to graphene sheets by the addition of agents such as amines, sodium borohydride, and ascorbic acid [129]. It is important to note that detrimental defects in the graphene sheets may arise as a result of long exposure time and high power ultrasonication. In addition to that, formation of chemical bonds between TiO_2 and graphene may be difficult due to the mild operating conditions [130]. Nonetheless, this technique provides the benefit of uniformly distributing the TiO_2 nanoparticles over the graphene sheets, ultimately improving the photocatalyst's activity [129].

Self-assembly is also another highly efficient, time-saving and cost effective synthesis technique [134,135]. This method offers structure and size control via component design and is applicable in various fields. The major disadvantages include the need for surfactants, sensitivity to environmental factors and production of graphene with low mechanical strength [136]. Surfactants are required in order to help disperse graphene oxide sheets and in order to improve TiO_2 nanoparticle loading [132]. Self-assembly based on the electrostatic attraction between negatively charged graphene oxide sheets and positively charged TiO_2 nanoparticles has been used to synthesize layered graphene-based TiO_2 semiconductors in a simple and cost-effective manner [132,137].

Tu et al. [138] loaded TiO_2 nanoparticles onto graphene nanosheets via an in situ method. The addition of graphene significantly increased the specific surface area of the catalyst, consequently generating more adsorption and reaction sites on the catalytic surface. The 2 wt.% graphene/TiO_2 catalyst was used to reduce CO_2 to ethane with a yield of 16.8 μmol/g-cat/h. Ong et al. [105] deposited nitrogen-doped TiO_2 nanoparticles onto graphene sheets using a solvothermal method. The nitrogen-doped TiO_2/graphene catalyst reduced CO_2 to methane with a yield of 0.37 μmol/g-cat/h. The efficient charge separation of graphene and the enhanced absorption of visible light were attributed to the improved photocatalytic performance of TiO_2.

3.4. Heterostructures

Sensitizing wide bandgap semiconductors with narrow bandgap semiconductors or dye molecules to form heterostructures is another method used to improve the photoactivity of many photocatalysts. This strategy provides means of increasing absorption toward the visible light region, at the same time enhancing the electron–hole pair separation, setting apart the reduction and oxidation sites for an improved performance [40,139]. Examples of narrow bandgap semiconductors that have been coupled with TiO_2 for photocatalytic reduction of CO_2 under visible light irradiation include CdS [140], Bi_2S_3 [141], CdSe quantum dots (QDs) [142], PbS QDs [143], and AgBr [144]. To enhance the adsorption of CO_2 molecules, materials with high intrinsic basicity, such as cobalt aluminum hydroxide, can be applied as sensitizers of TiO_2 [145]. Four different types of heterostructures exist depending on the charge carrier separation mechanism: conventional type-II, p-n, direct Z-scheme and surface heterojunction. However, these mechanisms will not be further discussed as they are considered to be outside the scope of this review. More details may be found elsewhere [40,146,147].

To synthetize heterostructured photocatalysts, several fabrication methods, including chemical vapor deposition, atomic layer deposition, hydrothermal/solvothermal, and ion exchange reactions, have been developed [147]. Chemical vapor deposition allows for the sequential deposition of multiple materials on a substrate surface. This synthesis route follows a two-step growth procedure: (1) growth of inner core semiconductor on a suitable substrate, and (2) deposition of outer layer shell semiconductor on the core surface. Compared to chemical vapor deposition, atomic layer deposition is usually more favored due to its enhanced benefits which include precise control of film thickness at the atomic level and conformal growth of complex nanostructures [148,149]. Studies have also shown that atomic layer deposition enhances the light trapping and carrier separation properties of the photocatalytic heterostructure [150,151]. A more convenient preparation technique is the hydrothermal/solvothermal

method. Both the precursor dissolution and the reaction rate are enhanced by this process. Ion exchange is another approach used to synthesize photocatalytic heterostructures. In this novel process, cations at the interface of the two semiconducting materials are exchanged [152,153]. Without changing the shape of the ionic semiconductor, ion exchange reactions selectively yield a dimer structure with an epitaxial hetero-interface [147].

Li et al. [141] prepared a Bi_2S_3/TiO_2 nanotube heterostructure for the photocatalytic reduction of CO_2 into methanol. The incorporation of Bi_2S_3 enhanced the visible light absorption and the photocatalytic performance of the TiO_2 nanotubes. The methanol yield of the Bi_2S_3/TiO_2 nanotube heterostructure was reported to be 44.92 μmol/g-cat/h. Qin et al. [38] investigated the conversion of CO_2 to methyl formate on a CuO-TiO_2 heterostructured composite in methanol. The photocatalytic activity was greatly enhanced due to the heterojunction between CuO and TiO_2. More specifically, the surface-junction improved the transfer of charges by facilitating the migration of electrons from the TiO_2 CB to the CuO VB as depicted in Figure 13a. Consequently, the probability of charge recombination was lowered and the photocatalytic efficiency was enhanced. As can be seen in Figure 13b, the TiO_2 catalyst loaded with 1 wt.% CuO exhibited the highest methyl formate yield of 1602 μmol/g-cat/h. One of the most significant approaches was carried out by Nguyen et al. [154], who employed a metal doped TiO_2 catalyst sensitized with ruthenium dye (N3 dye) for the photoreduction of CO_2 into methane. The methane yield of the N3-Dye-Cu (0.5 wt.%)-Fe (0.5 wt.%)/TiO_2 was 0.617 μmol/g-cat/h. The improved photoreduction of the dye-sensitized TiO_2 is attributed to the full absorption of visible light by the N3-dye along with the efficient charge transfer in the N3 dye-TiO_2 system.

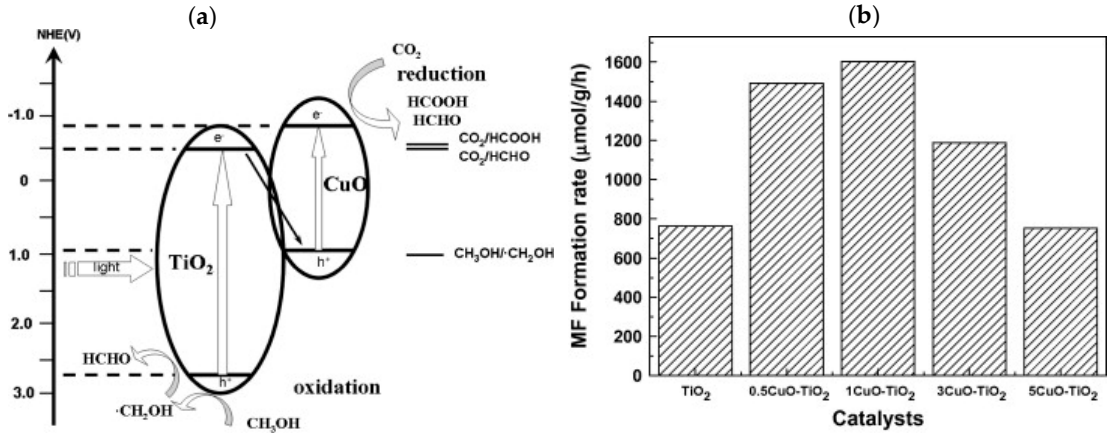

Figure 13. Photocatalytic conversion of CO_2 to methyl formate (MF) over CuO–TiO_2. (**a**) Band positions of CuO and TiO_2. (**b**) Formation rate of MF for the different catalysts. Reproduced from work in [38]. Copyright 2010 Elsevier Inc.

3.5. Dispersion on Supports

The dispersion of TiO_2 as a nanoparticle on various types of supports enhances the catalyst's product selectivity, pore structure, and electronic properties. In addition to that, this modification technique eliminates the need for post treatment separation and provides high surface area and mass transfer rate. An ideal supported-TiO_2 photocatalyst must have effective light absorption properties, be resistant to degradation induced by the immobilization technique and provide firm adhesion between the support and the catalyst. Key challenges of this strategy include mass transfer limitations and low light utilization efficiency. TiO_2 photocatalysts may be immobilized by dip or spin coating onto substrates such as fibers, membranes, glass, monolithic ceramics, silica, and clays. In dip coating, the thoroughly cleaned supports are immersed in a coating precursor solution as is demonstrated in Figure 14a. After being slowly pulled out of the solution, the coated support is then dried out to remove excess solution and moisture [155]. The withdrawal speed of the substrate, number of coating cycles and the TiO_2 solution viscosity determine the catalyst film thickness [23]. In spin coating, the

precursor is deposited on the substrate by a dispenser while the substrate is rotated as demonstrated in Figure 14b. The rotation continues until uniform distribution of the precursor layer is achieved. Although the spinning process will result in the partial evaporation of the precursor solvent, the substrate will still require additional thermal treatment to stabilize the layer. The thickness of the films obtained by spin coating depends on the concentration of the precursor solution and the rotation speed [156]. Due to its scale-up applicability and higher controllability, dip coating is usually preferred over the spin coating technique [157]. In addition to that, superior structural and optical properties, such as enhanced crystallinity and higher average particle size, have been observed for dip-coated films in comparison to spin-coated ones [158,159].

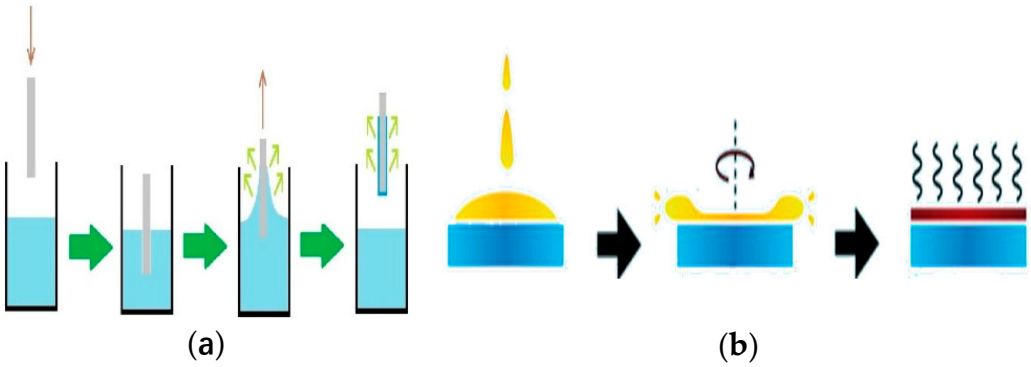

Figure 14. Dip-coating (**a**) and spin-coating (**b**) of TiO_2 photocatalyst on an inert support. Reproduced from work in [155,160]. Copyright 2017 Elsevier Ltd., 2016 Elsevier B.V.

Bellardita et al. [87] investigated the photocatalytic activity of silica-supported TiO_2 for the reduction of CO_2. The primary product obtained from the photocatalytic reaction was acetaldehyde. Li et al. [106] prepared an ordered mesoporous silica-supported Cu/TiO_2 nanocomposites via a sol–gel method for the photocatalytic reduction of CO_2 in water under UV irradiation (Figure 15a). As previously discussed, one of the many benefits of sol–gel synthesis concerns the control of pore size and the pore size distribution of the final catalyst. The sol–gel method used to prepare the silica-supported Cu/TiO_2 was carefully formulated to produce ordered mesoporous silica with a pore size of ~15 nm [161]. The ordered mesoporous structure of silica was clearly observed in transmission electron microscopy (TEM) images as shown in Figure 15c,d. Mesoporous silica, with its ordered pore networks, has a much higher surface area than agglomerates of silica nanoparticles with irregular mesopores and is therefore considered a better support for catalysts. The high surface area of the ordered mesoporous silica support (>300 m^2/g) enhanced the dispersion of TiO_2 nanoparticles and improved the adsorption of reactants on the catalytic surface. The main product of the CO_2 photoreduction reaction was carbon monoxide when bare TiO_2 was supported on silica. However, when Cu/TiO_2 was supported on silica, the production rate of methane significantly increased. The deposition of Cu enhanced the separation of charges and improved the kinetics of the multi-electron reactions, consequently increasing methane selectivity. As can be deduced from Figure 15b, the 0.5 wt.% Cu/TiO_2-Silica composite produced carbon monoxide and methane with a yield of 60 and 10 μmol/g-cat/h, respectively.

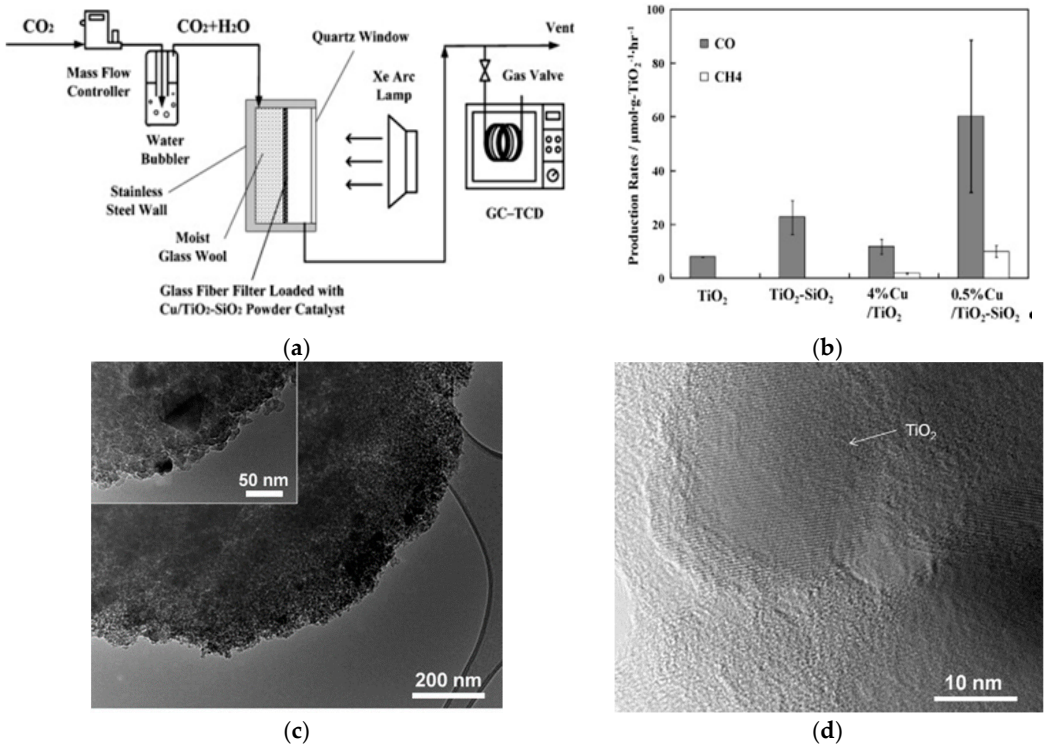

Figure 15. Photocatalytic reduction of CO_2 on ordered mesoporous silica supported Cu/TiO_2. (**a**) Schematic representation of experimental set-up; (**b**) production rates of CO and methane; (**c**) transmission electron microscopy (TEM) image of the 0.5 wt.% Cu/TiO_2-Silica composite; (**d**) high resolution TEM image of a single TiO_2 nanoparticle. Reproduced from work in [106]. Copyright 2010 Elsevier B.V.

4. Conclusions and Future Perspective

In this review, recent advances in the area of CO_2 photoreduction have been discussed and the basic mechanism of CO_2 photoreduction, particularly with water, has been described. Limited studies exist on the reaction mechanism and kinetics of CO_2 photoreduction as a result of the complexity of the reaction which is due mainly to the possibility of forming various products and the presence of many reaction pathways. In situ techniques, such as FTIR and NMR, would help investigate crucial reaction kinetic parameters such as active sites, electronic states and reaction intermediates. Additionally, various modification strategies of TiO_2 that may help overcome the limitations of current CO_2 photoreduction technologies have been described. A comparative assessment between the different TiO_2-based catalysts that have been reported in literature so far for CO_2 photoreduction was made. This overview of the latest research trends in CO_2 photoreduction may be used as a tool to help develop low-cost and highly-efficient TiO_2-based semiconductors for an improved photocatalytic reduction of CO_2.

Regardless of the significant theoretical advancements, the practical application of TiO_2 photocatalysts for the photoreduction of CO_2 is still far from being attained. This is mainly due to the lack of stable and visible light active photocatalysts. Researchers must focus on engineering a photocatalytic nanocomposite with an optimum band gap that simultaneously enhances charge separation and visible light absorption. A few suggested strategies include coupling wide band gap semiconductors with narrow ones, introduction of oxygen vacancies and defect sites and functionalization of the TiO_2 surface. To enhance the adsorption and reduction of CO_2 especially in the presence of water, a basic and hydrophobic TiO_2 surface must be developed. The latest studies clearly demonstrate the considerable improvement in the yield and efficiency of the CO_2 photoreduction process with modified TiO_2 catalysts. More specifically, the major limitations of TiO_2, including weak visible light absorption,

increased charge recombination, and low CO_2 adsorption capacity, have been greatly overcome by synthesizing nanocomposites with exposed reactive sites and improved morphology.

Surface modifications to TiO_2-based photocatalysts cannot solely suffice the technical and economic feasibility requirements of CO_2 photoreduction applications, especially if they are to be applied on a large industrial scale. One promising solution could be to combine photocatalysis with other CO_2 conversion methods such as thermochemical and/or electrochemical catalysis. Another suggested solution could be to couple modified TiO_2 with other visible-light active photocatalysts with the aim of improving the photocatalytic process under solar irradiation. Further enhancement might be attained if compressed CO_2 (liquid or supercritical) is used for the photocatalytic reduction process. Although this increases the CO_2 conversion efficiency, the overall cost will be considerably high due to intensive compression requirements. In this case, industries already utilizing compressed CO_2 must be targeted.

Funding: We acknowledge financial support from Khalifa University of Science and Technology through the Research and Innovation Center on CO_2 and H_2 (RICH) (grant RC2-2019-007). We also acknowledge financial support from Abu Dhabi Education and Knowledge through the Award for Research Excellence (grant AARE17-8434000095).

Conflicts of Interest: The authors declare no conflict of interest.

References

1. Ryaboshapko, A.G.; Revokatova, A.P. A potential role of the negative emission of carbon dioxide in solving the climate problem. *Russ. Meteorol. Hydrol.* **2015**, *40*, 443–455. [CrossRef]
2. Nordhaus, W.D. *The Climate Casino: Risk, Uncertainty, and Economics for a Warming World*; Yale University Press: New Haven, CT, USA, 2013.
3. Gore, A. The Crisis Comes Ashore. *New Repub.* **2010**, *241*, 10–12.
4. Shin, D.Y.; Jo, J.H.; Lee, J.-Y.; Lim, D.-H. Understanding mechanisms of carbon dioxide conversion into methane for designing enhanced catalysts from first-principles. *Comput. Chem.* **2016**, *1083*, 31–37. [CrossRef]
5. Holdren, J.P. Population and the energy problem. *Popul. Environ.* **1991**, *12*, 231–255. [CrossRef]
6. Sanchez, J.A. *Carbon Dioxide Capture: Processes, Technology and Environmental Implications*; Nova Science Publishers, Inc.: Hauppauge, NY, USA, 2016.
7. Spigarelli, B.P.; Kawatra, S.K. Opportunities and challenges in carbon dioxide capture. *J. Co2 Util.* **2013**, *1*, 69–87. [CrossRef]
8. Cheah, W.Y.; Ling, T.C.; Juan, J.C.; Lee, D.-J.; Chang, J.-S.; Show, P.L. Biorefineries of carbon dioxide: From carbon capture and storage (CCS) to bioenergies production. *Bioresour. Technol.* **2016**, *215*, 346–356. [CrossRef]
9. Koytsoumpa, E.I.; Bergins, C.; Kakaras, E. The CO_2 economy: Review of CO_2 capture and reuse technologies. *J. Supercrit. Fluids* **2018**, *132*, 3–16. [CrossRef]
10. Sahebdelfar, S.; Takht Ravanchi, M. Carbon dioxide utilization for methane production: A thermodynamic analysis. *J. Pet. Sci. Eng.* **2015**, *134*, 14–22. [CrossRef]
11. Centi, G.; Perathoner, S. Opportunities and prospects in the chemical recycling of carbon dioxide to fuels. *Catal. Today* **2009**, *148*, 191–205. [CrossRef]
12. Muradov, N. Industrial Utilization of CO_2: A Win–Win Solution. In *Liberating Energy from Carbon: Introduction to Decarbonization*; Springer: New York, NY, USA, 2014; pp. 325–383. [CrossRef]
13. Ganesh, I. Conversion of carbon dioxide into methanol—A potential liquid fuel: Fundamental challenges and opportunities (a review). *Renew. Sustain. Energy Rev.* **2014**, *31*, 221–257. [CrossRef]
14. Arakawa, H.; Aresta, M.; Armor, J.N.; Barteau, M.A.; Beckman, E.J.; Bell, A.T.; Bercaw, J.E.; Creutz, C.; Dinjus, E.; Dixon, D.A.; et al. Catalysis Research of Relevance to Carbon Management: Progress, Challenges, and Opportunities. *Chem. Rev.* **2001**, *101*, 953–996. [CrossRef]
15. Liu, X.-M.; Lu, G.Q.; Yan, Z.-F.; Beltramini, J. Recent Advances in Catalysts for Methanol Synthesis via Hydrogenation of CO and CO_2. *Ind. Eng. Chem. Res.* **2003**, *42*, 6518–6530. [CrossRef]
16. Farrelly, D.J.; Everard, C.D.; Fagan, C.C.; McDonnell, K.P. Carbon sequestration and the role of biological carbon mitigation: A review. *Renew. Sustain. Energy Rev.* **2013**, *21*, 712–727. [CrossRef]
17. Alaswad, A.; Dassisti, M.; Prescott, T.; Olabi, A.G. Technologies and developments of third generation biofuel production. *Renew. Sustain. Energy Rev.* **2015**, *51*, 1446–1460. [CrossRef]

18. Ramachandriya, K.D.; Kundiyana, D.K.; Wilkins, M.R.; Terrill, J.B.; Atiyeh, H.K.; Huhnke, R.L. Carbon dioxide conversion to fuels and chemicals using a hybrid green process. *Appl. Energy* **2013**, *112*, 289–299. [CrossRef]
19. de_Richter, R.K.; Ming, T.; Caillol, S. Fighting global warming by photocatalytic reduction of CO_2 using giant photocatalytic reactors. *Renew. Sustain. Energy Rev.* **2013**, *19*, 82–106. [CrossRef]
20. Hoffmann, M.R.; Moss, J.A.; Baum, M.M. Artificial photosynthesis: Semiconductor photocatalytic fixation of CO_2 to afford higher organic compounds. *Dalton Trans.* **2011**, *40*, 5151–5158. [CrossRef]
21. Kočí, K.; Obalová, L.; Lacný, Z. Photocatalytic reduction of CO_2 over TiO_2 based catalysts. *Chem. Pap.* **2008**, *62*, 1–9. [CrossRef]
22. Habisreutinger, S.N.; Schmidt-Mende, L.; Stolarczyk, J.K. Photocatalytic reduction of CO_2 on TiO_2 and other semiconductors. *Angew. Chem. Int. Ed.* **2013**, *52*, 7372–7408. [CrossRef]
23. Ola, O.; Maroto-Valer, M.M. Review of material design and reactor engineering on TiO_2 photocatalysis for CO_2 reduction. *J. Photochem. Photobiol. C* **2015**, *24*, 16–42. [CrossRef]
24. Kumar, A.; Ashok, A.; Shurair, M.S.; Yussuf, K.; van den Broeke, L.J. Carbon Management: Regional Solutions Based on Carbon Dioxide Utilization and Process Integration. In Proceedings of the 4th International Gas Processing Symposium, Doha, Qatar, 26–27 October 2014; Elsevier: Oxford, UK, 2015.
25. Li, K.; An, X.; Park, K.H.; Khraisheh, M.; Tang, J. A critical review of CO_2 photoconversion: Catalysts and reactors. *Catal. Today* **2014**, *224*, 3–12. [CrossRef]
26. Meryem, S.S.; Nasreen, S.; Siddique, M.; Khan, R. An overview of the reaction conditions for an efficient photoconversion of CO_2. *Rev. Chem. Eng.* **2018**, *34*, 409–425. [CrossRef]
27. Mallouk, T.E. The Emerging Technology of Solar Fuels. *J. Phys. Chem. Lett.* **2010**, *1*, 2738–2739. [CrossRef]
28. Shi, R.; Waterhouse, G.I.N.; Zhang, T. Recent Progress in Photocatalytic CO_2 Reduction Over Perovskite Oxides. *Sol. Rrl* **2017**, *1*, 1700126. [CrossRef]
29. AlOtaibi, B.; Fan, S.; Wang, D.; Ye, J.; Mi, Z. Wafer-level artificial photosynthesis for CO_2 reduction into CH_4 and CO using GaN nanowires. *ACS Catal.* **2015**, *5*, 5342–5348. [CrossRef]
30. Zhang, Y.; Xu, C.; Chen, J.; Zhang, X.; Wang, Z.; Zhou, J.; Cen, K. A novel photo-thermochemical cycle for the dissociation of CO_2 using solar energy. *Appl. Energy* **2015**, *156*, 223–229. [CrossRef]
31. Wang, P.; Wang, S.; Wang, H.; Wu, Z.; Wang, L. Recent Progress on Photo-Electrocatalytic Reduction of Carbon Dioxide. *Part. Part. Syst. Char.* **2018**, *35*, 1700371. [CrossRef]
32. Halmann, M. Photoelectrochemical reduction of aqueous carbon dioxide on p-type gallium phosphide in liquid junction solar cells. *Nature* **1978**, *275*, 115–116. [CrossRef]
33. Kumar, S.G.; Devi, L.G. Review on Modified TiO_2 Photocatalysis under UV/Visible Light: Selected Results and Related Mechanisms on Interfacial Charge Carrier Transfer Dynamics. *J. Phys. Chem. A* **2011**, *115*, 13211–13241. [CrossRef]
34. Daghrir, R.; Drogui, P.; Robert, D. Modified TiO_2 For Environmental Photocatalytic Applications: A Review. *Ind. Eng. Chem. Res.* **2013**, *52*, 3581–3599. [CrossRef]
35. Wen, J.; Li, X.; Liu, W.; Fang, Y.; Xie, J.; Xu, Y. Photocatalysis fundamentals and surface modification of TiO_2 nanomaterials. *Chin. J. Catal.* **2015**, *36*, 2049–2070. [CrossRef]
36. Li, X.; Zhuang, Z.; Li, W.; Pan, H. Photocatalytic reduction of CO_2 over noble metal-loaded and nitrogen-doped mesoporous TiO_2. *Appl. Catal. A* **2012**, *429–430*, 31–38. [CrossRef]
37. Corma, A.; Garcia, H. Photocatalytic reduction of CO_2 for fuel production: Possibilities and challenges. *J. Catal.* **2013**, *308*, 168–175. [CrossRef]
38. Qin, S.; Xin, F.; Liu, Y.; Yin, X.; Ma, W. Photocatalytic reduction of CO_2 in methanol to methyl formate over CuO–TiO_2 composite catalysts. *J. Colloid Interface Sci.* **2011**, *356*, 257–261. [CrossRef]
39. Karamian, E.; Sharifnia, S. On the general mechanism of photocatalytic reduction of CO_2. *J. Co2 Util.* **2016**, *16*, 194–203. [CrossRef]
40. Low, J.; Cheng, B.; Yu, J. Surface modification and enhanced photocatalytic CO_2 reduction performance of TiO_2: A review. *Appl. Surf. Sci.* **2017**, *392*, 658–686. [CrossRef]
41. Dilla, M.; Schlögl, R.; Strunk, J. Photocatalytic CO_2 Reduction Under Continuous Flow High-Purity Conditions: Quantitative Evaluation of CH4 Formation in the Steady-State. *ChemCatChem* **2017**, *9*, 696–704. [CrossRef]
42. Mino, L.; Spoto, G.; Ferrari, A.M. CO_2 capture by TiO_2 anatase surfaces: A combined DFT and FTIR study. *J. Phys. Chem. C* **2014**, *118*, 25016–25026. [CrossRef]

43. Sorescu, D.C.; Al-Saidi, W.A.; Jordan, K.D. CO_2 adsorption on TiO_2 (101) anatase: A dispersion-corrected density functional theory study. *J. Chem. Phys.* **2011**, *135*, 124701. [CrossRef]
44. Tu, W.; Zhou, Y.; Zou, Z. Photocatalytic conversion of CO_2 into renewable hydrocarbon fuels: State-of-the-art accomplishment, challenges, and prospects. *Adv. Mater.* **2014**, *26*, 4607–4626. [CrossRef]
45. Yuan, L.; Xu, Y.-J. Photocatalytic conversion of CO_2 into value-added and renewable fuels. *Appl. Surf. Sci.* **2015**, *342*, 154–167. [CrossRef]
46. Halmann, M. 15—Photochemical Fixation of Carbon Dioxide. In *Energy Resources Through Photochemistry and Catalysis*; Grätzel, M., Ed.; Academic Press: Cambridge, MA, USA, 1983; pp. 507–534. Available online: https://linkinghub.elsevier.com/retrieve/pii/B9780122957208500193 (accessed on 1 December 2019). [CrossRef]
47. Tan, L.-L.; Ong, W.-J.; Chai, S.-P.; Mohamed, A.R. Photocatalytic reduction of CO_2 with H_2O over graphene oxide-supported oxygen-rich TiO_2 hybrid photocatalyst under visible light irradiation: Process and kinetic studies. *Chem. Eng. J.* **2017**, *308*, 248–255. [CrossRef]
48. Liu, L.; Li, Y. Understanding the reaction mechanism of photocatalytic reduction of CO_2 with H_2O on TiO_2-based photocatalysts: A review. *Aerosol Air Qual. Res.* **2014**, *14*, 453–469. [CrossRef]
49. Uner, D.; Oymak, M.M. On the mechanism of photocatalytic CO_2 reduction with water in the gas phase. *Catal. Today* **2012**, *181*, 82–88. [CrossRef]
50. Saladin, F.; Alxneit, I. Temperature dependence of the photochemical reduction of CO_2 in the presence of H_2 Oat the solid/gas interface of TiO_2. *J. Chem. Soc. Faraday Trans.* **1997**, *93*, 4159–4163. [CrossRef]
51. Handoko, A.D.; Li, K.; Tang, J. Recent progress in artificial photosynthesis: CO_2 photoreduction to valuable chemicals in a heterogeneous system. *Curr. Opin. Chem. Eng.* **2013**, *2*, 200–206. [CrossRef]
52. Subrahmanyam, M.; Kaneco, S.; Alonso-Vante, N. A screening for the photo reduction of carbon dioxide supported on metal oxide catalysts for C1–C3 selectivity. *Appl. Catal. B* **1999**, *23*, 169–174. [CrossRef]
53. Sasirekha, N.; Basha, S.J.S.; Shanthi, K. Photocatalytic performance of Ru doped anatase mounted on silica for reduction of carbon dioxide. *Appl. Catal. B* **2006**, *62*, 169–180. [CrossRef]
54. Akhter, P.; Hussain, M.; Saracco, G.; Russo, N. Novel nanostructured-TiO_2 materials for the photocatalytic reduction of CO_2 greenhouse gas to hydrocarbons and syngas. *Fuel* **2015**, *149*, 55–65. [CrossRef]
55. Klyukin, K.; Alexandrov, V. CO_2 Adsorption and Reactivity on Rutile TiO_2(110) in Water: An Ab Initio Molecular Dynamics Study. *J. Phys. Chem. C* **2017**, *121*, 10476–10483. [CrossRef]
56. Liu, B.-J.; Torimoto, T.; Matsumoto, H.; Yoneyama, H. Effect of solvents on photocatalytic reduction of carbon dioxide using TiO_2 nanocrystal photocatalyst embedded in SiO_2 matrices. *J. Photochem. Photobiol. A* **1997**, *108*, 187–192. [CrossRef]
57. Kočí, K.; Obalová, L.; Matějová, L.; Plachá, D.; Lacný, Z.; Jirkovský, J.; Šolcová, O. Effect of TiO_2 particle size on the photocatalytic reduction of CO_2. *Appl. Catal. B* **2009**, *89*, 494–502. [CrossRef]
58. Tseng, I.-H.; Chang, W.-C.; Wu, J.C. Photoreduction of CO_2 using sol–gel derived titania and titania-supported copper catalysts. *Appl. Catal. B* **2002**, *37*, 37–48. [CrossRef]
59. Sastre, F.; Corma, A.; García, H. 185 nm Photoreduction of CO_2 to Methane by Water. Influence of the Presence of a Basic Catalyst. *J. Am. Chem. Soc.* **2012**, *134*, 14137–14141. [CrossRef] [PubMed]
60. Lo, C.-C.; Hung, C.-H.; Yuan, C.-S.; Wu, J.-F. Photoreduction of carbon dioxide with H_2 and H_2O over TiO_2 and ZrO_2 in a circulated photocatalytic reactor. *Sol. Energy Mater. Sol. Cells* **2007**, *91*, 1765–1774. [CrossRef]
61. Grills, D.C.; Fujita, E. New directions for the photocatalytic reduction of CO_2: Supramolecular, $scCO_2$ or biphasic ionic liquid—$scCO_2$ systems. *J. Phys. Chem. Lett.* **2010**, *1*, 2709–2718. [CrossRef]
62. Kaneco, S.; Kurimoto, H.; Ohta, K.; Mizuno, T.; Saji, A. Photocatalytic reduction of CO_2 using TiO_2 powders in liquid CO_2 medium. *J. Photochem. Photobiol. A* **1997**, *109*, 59–63. [CrossRef]
63. Kaneco, S.; Kurimoto, H.; Shimizu, Y.; Ohta, K.; Mizuno, T. Photocatalytic reduction of CO_2 using TiO_2 powders in supercritical fluid CO_2. *Energy* **1999**, *24*, 21–30. [CrossRef]
64. Kometani, N.; Hirata, S.; Chikada, M. Photocatalytic reduction of CO_2 by Pt-loaded TiO_2 in the mixture of sub-and supercritical water and CO_2. *J. Supercrit. Fluids* **2017**, *120*, 443–447. [CrossRef]
65. Liu, L.; Zhao, H.; Andino, J.M.; Li, Y. Photocatalytic CO_2 reduction with H_2O on TiO_2 nanocrystals: Comparison of anatase, rutile, and brookite polymorphs and exploration of surface chemistry. *ACS Catal.* **2012**, *2*, 1817–1828. [CrossRef]

66. Chen, L.; Graham, M.E.; Li, G.; Gentner, D.R.; Dimitrijevic, N.M.; Gray, K.A. Photoreduction of CO_2 by TiO_2 nanocomposites synthesized through reactive direct current magnetron sputter deposition. *Thin Solid Film.* **2009**, *517*, 5641–5645. [CrossRef]
67. Haggerty, J.E.S.; Schelhas, L.T.; Kitchaev, D.A.; Mangum, J.S.; Garten, L.M.; Sun, W.; Stone, K.H.; Perkins, J.D.; Toney, M.F.; Ceder, G.; et al. High-fraction brookite films from amorphous precursors. *Sci. Rep.* **2017**, *7*, 15232. [CrossRef] [PubMed]
68. Zhang, P.; Tang, B.; Xia, W.; Wang, F.; Wei, X.; Xiang, J.; Li, J. Preparation and Characterizations of TiO_2 Nanoparticles by Sol-Gel Process using DMAC Solvent. *MMECEB* **2015**, *2016*, 892–895.
69. Akpan, U.; Hameed, B. The advancements in sol–gel method of doped-TiO_2 photocatalysts. *Appl. Catal. A* **2010**, *375*, 1–11. [CrossRef]
70. Wang, Y.; He, Y.; Lai, Q.; Fan, M. Review of the progress in preparing nano TiO_2: An important environmental engineering material. *J. Environ. Sci.* **2014**, *26*, 2139–2177. [CrossRef] [PubMed]
71. Chen, Y.; Lunsford, S.K.; Song, Y.; Ju, H.; Falaras, P.; likodimos, V.; Kontos, A.G.; Dionysiou, D.D. Synthesis, characterization and electrochemical properties of mesoporous zirconia nanomaterials prepared by self-assembling sol–gel method with Tween 20 as a template. *Chem. Eng. J.* **2011**, *170*, 518–524. [CrossRef]
72. Sun, Y.; Seo, J.H.; Takacs, C.J.; Seifter, J.; Heeger, A.J. Inverted polymer solar cells integrated with a low-temperature-annealed sol-gel-derived ZnO film as an electron transport layer. *Adv. Mater.* **2011**, *23*, 1679–1683. [CrossRef]
73. Djaoued, Y.; Balaji, S.; Beaudoin, N. Sol–gel synthesis of mesoporous WO3–TiO_2 composite thin films for photochromic devices. *J. Sol-Gel Sci. Technol.* **2013**, *65*, 374–383. [CrossRef]
74. Chen, C.; Cai, W.; Long, M.; Zhang, J.; Zhou, B.; Wu, Y.; Wu, D. Template-free sol–gel preparation and characterization of free-standing visible light responsive C, N-modified porous monolithic TiO_2. *J. Hazard. Mater.* **2010**, *178*, 560–565. [CrossRef]
75. Tseng, T.K.; Lin, Y.S.; Chen, Y.J.; Chu, H. A review of photocatalysts prepared by sol-gel method for VOCs removal. *Int. J. Mol. Sci.* **2010**, *11*, 2336–2361. [CrossRef]
76. Lu, J.; Li, L.; Wang, Z.; Wen, B.; Cao, J. Synthesis of visible-light-active TiO_2-based photo-catalysts by a modified sol–gel method. *Mater. Lett.* **2013**, *94*, 147–149. [CrossRef]
77. You, Y.; Zhang, S.; Wan, L.; Xu, D. Preparation of continuous TiO_2 fibers by sol–gel method and its photocatalytic degradation on formaldehyde. *Appl. Surf. Sci.* **2012**, *258*, 3469–3474. [CrossRef]
78. Xie, Y.; Zhao, Q.; Zhao, X.J.; Li, Y. Low temperature preparation and characterization of N-doped and NS-codoped TiO_2 by sol–gel route. *Catal. Lett.* **2007**, *118*, 231–237. [CrossRef]
79. Šegota, S.; Ćurković, L.; Ljubas, D.; Svetličić, V.; Houra, I.F.; Tomašić, N. Synthesis, characterization and photocatalytic properties of sol–gel TiO_2 films. *Ceram. Int.* **2011**, *37*, 1153–1160. [CrossRef]
80. Kim, M.-S.; Liu, G.; Nam, W.K.; Kim, B.-W. Preparation of porous carbon-doped TiO_2 film by sol–gel method and its application for the removal of gaseous toluene in the optical fiber reactor. *J. Ind. Eng. Chem.* **2011**, *17*, 223–228. [CrossRef]
81. Macwan, D.; Dave, P.N.; Chaturvedi, S. A review on nano-TiO_2 sol–gel type syntheses and its applications. *Asian J. Mater. Sci.* **2011**, *46*, 3669–3686. [CrossRef]
82. Payakgul, W.; Mekasuwandumrong, O.; Pavarajarn, V.; Praserthdam, P. Effects of reaction medium on the synthesis of TiO_2 nanocrystals by thermal decomposition of titanium (IV) n-butoxide. *Ceram. Int.* **2005**, *31*, 391–397. [CrossRef]
83. Liu, Z.; Sun, D.D.; Guo, P.; Leckie, J.O. One-step fabrication and high photocatalytic activity of porous TiO_2 hollow aggregates by using a low-temperature hydrothermal method without templates. *Chem. Eur. J.* **2007**, *13*, 1851–1855. [CrossRef]
84. Ou, H.-H.; Lo, S.-L. Review of titania nanotubes synthesized via the hydrothermal treatment: Fabrication, modification, and application. *Sep. Purif. Technol.* **2007**, *58*, 179–191. [CrossRef]
85. Fumin, W.; Zhansheng, S.; Feng, G.; Jinting, J.; Adachi, M. Morphology control of anatase TiO_2 by surfactant-assisted hydrothermal method. *Chin. J. Chem. Eng.* **2007**, *15*, 754–759.
86. Camarillo, R.; Tostón, S.; Martínez, F.; Jiménez, C.; Rincón, J. Preparation of TiO_2-based catalysts with supercritical fluid technology: Characterization and photocatalytic activity in CO_2 reduction. *J. Chem. Technol. Biotechnol.* **2017**, *92*, 1710–1720. [CrossRef]

87. Bellardita, M.; Di Paola, A.; García-López, E.; Loddo, V.; Marcì, G.; Palmisano, L. Photocatalytic CO_2 reduction in gas-solid regime in the presence of bare, SiO_2 supported or Cu-loaded TiO_2 samples. *Curr. Org. Chem.* **2013**, *17*, 2440–2448. [CrossRef]
88. Maeda, K. Photocatalytic water splitting using semiconductor particles: History and recent developments. *J. Photochem. Photobiol. C* **2011**, *12*, 237–268. [CrossRef]
89. Humayun, M.; Raziq, F.; Khan, A.; Luo, W. Modification strategies of TiO_2 for potential applications in photocatalysis: A critical review. *Green Chem. Lett. Rev.* **2018**, *11*, 86–102. [CrossRef]
90. Meng, X.; Ouyang, S.; Kako, T.; Li, P.; Yu, Q.; Wang, T.; Ye, J. Photocatalytic CO_2 conversion over alkali modified TiO_2 without loading noble metal cocatalyst. *Chem. Commun.* **2014**, *50*, 11517–11519. [CrossRef]
91. Wang, W.-N.; An, W.-J.; Ramalingam, B.; Mukherjee, S.; Niedzwiedzki, D.M.; Gangopadhyay, S.; Biswas, P. Size and structure matter: Enhanced CO_2 photoreduction efficiency by size-resolved ultrafine Pt nanoparticles on TiO_2 single crystals. *J. Am. Chem. Soc.* **2012**, *134*, 11276–11281. [CrossRef]
92. Tahir, M.; Tahir, B.; Amin, N.A.S. Gold-nanoparticle-modified TiO_2 nanowires for plasmon-enhanced photocatalytic CO_2 reduction with H_2 under visible light irradiation. *Appl. Surf. Sci.* **2015**, *356*, 1289–1299. [CrossRef]
93. Kong, D.; Tan, J.Z.Y.; Yang, F.; Zeng, J.; Zhang, X. Electrodeposited Ag nanoparticles on TiO_2 nanorods for enhanced UV visible light photoreduction CO_2 to CH4. *Appl. Surf. Sci.* **2013**, *277*, 105–110. [CrossRef]
94. Zhai, Q.; Xie, S.; Fan, W.; Zhang, Q.; Wang, Y.; Deng, W.; Wang, Y. Photocatalytic conversion of carbon dioxide with water into methane: Platinum and copper (I) oxide co-catalysts with a core–shell structure. *Angew. Chem.* **2013**, *125*, 5888–5891. [CrossRef]
95. Yan, Y.; Yu, Y.; Cao, C.; Huang, S.; Yang, Y.; Yang, X.; Cao, Y. Enhanced photocatalytic activity of TiO_2–Cu/C with regulation and matching of energy levels by carbon and copper for photoreduction of CO_2 into CH_4. *CrystEngComm* **2016**, *18*, 2956–2964. [CrossRef]
96. Wu, J.C.S.; Lin, H.-M.; Lai, C.-L. Photo reduction of CO_2 to methanol using optical-fiber photoreactor. *Appl. Catal. A* **2005**, *296*, 194–200. [CrossRef]
97. Nasution, H.W.; Purnama, E.; Kosela, S.; Gunlazuardi, J. Photocatalytic reduction of CO_2 on copper-doped Titania catalysts prepared by improved-impregnation method. *Catal. Commun.* **2005**, *6*, 313–319. [CrossRef]
98. Kwak, B.S.; Vignesh, K.; Park, N.-K.; Ryu, H.-J.; Baek, J.-I.; Kang, M. Methane formation from photoreduction of CO_2 with water using TiO_2 including Ni ingredient. *Fuel* **2015**, *143*, 570–576. [CrossRef]
99. Matějová, L.; Kočí, K.; Reli, M.; Čapek, L.; Hospodková, A.; Peikertová, P.; Matěj, Z.; Obalová, L.; Wach, A.; Kuśtrowski, P.; et al. Preparation, characterization and photocatalytic properties of cerium doped TiO_2: On the effect of Ce loading on the photocatalytic reduction of carbon dioxide. *Appl. Catal. B* **2014**, *152–153*, 172–183. [CrossRef]
100. Zhao, Z.; Fan, J.; Wang, J.; Li, R. Effect of heating temperature on photocatalytic reduction of CO_2 by N–TiO_2 nanotube catalyst. *Catal. Commun.* **2012**, *21*, 32–37. [CrossRef]
101. Xue, L.M.; Zhang, F.H.; Fan, H.J.; Bai, X.F. Preparation of C Doped TiO_2 Photocatalysts and their Photocatalytic Reduction of Carbon Dioxide. *Adv. Mater. Res.* **2011**, *183–185*, 1842–1846. [CrossRef]
102. Gui, M.M.; Chai, S.-P.; Xu, B.-Q.; Mohamed, A.R. Enhanced visible light responsive MWCNT/TiO_2 core–shell nanocomposites as the potential photocatalyst for reduction of CO_2 into methane. *Sol. Energy Mater. Sol. Cells* **2014**, *122*, 183–189. [CrossRef]
103. Xia, X.-H.; Jia, Z.-J.; Yu, Y.; Liang, Y.; Wang, Z.; Ma, L.-L. Preparation of multi-walled carbon nanotube supported TiO_2 and its photocatalytic activity in the reduction of CO_2 with H_2O. *Carbon* **2007**, *45*, 717–721. [CrossRef]
104. Ong, W.-J.; Gui, M.M.; Chai, S.-P.; Mohamed, A.R. Direct growth of carbon nanotubes on Ni/TiO_2 as next generation catalysts for photoreduction of CO_2 to methane by water under visible light irradiation. *RSC Adv.* **2013**, *3*, 4505–4509. [CrossRef]
105. Ong, W.-J.; Tan, L.-L.; Chai, S.-P.; Yong, S.-T.; Mohamed, A.R. Self-assembly of nitrogen-doped TiO_2 with exposed {001} facets on a graphene scaffold as photo-active hybrid nanostructures for reduction of carbon dioxide to methane. *Nano Res.* **2014**, *7*, 1528–1547. [CrossRef]
106. Li, Y.; Wang, W.-N.; Zhan, Z.; Woo, M.-H.; Wu, C.-Y.; Biswas, P. Photocatalytic reduction of CO_2 with H_2O on mesoporous silica supported Cu/TiO_2 catalysts. *Appl. Catal. B* **2010**, *100*, 386–392. [CrossRef]

107. Sakthivel, S.; Shankar, M.V.; Palanichamy, M.; Arabindoo, B.; Bahnemann, D.W.; Murugesan, V. Enhancement of photocatalytic activity by metal deposition: Characterisation and photonic efficiency of Pt, Au and Pd deposited on TiO_2 catalyst. *Wat. Res.* **2004**, *38*, 3001–3008. [CrossRef] [PubMed]
108. Tostón, S.; Camarillo, R.; Martínez, F.; Jiménez, C.; Rincón, J. Supercritical synthesis of platinum-modified titanium dioxide for solar fuel production from carbon dioxide. *Chin. J. Catal.* **2017**, *38*, 636–650. [CrossRef]
109. Khan, M.R.; Chuan, T.W.; Yousuf, A.; Chowdhury, M.; Cheng, C.K. Schottky barrier and surface plasmonic resonance phenomena towards the photocatalytic reaction: Study of their mechanisms to enhance photocatalytic activity. *Catal. Sci. Technol.* **2015**, *5*, 2522–2531. [CrossRef]
110. Murakami, N.; Saruwatari, D.; Tsubota, T.; Ohno, T. Photocatalytic reduction of carbon dioxide over shape-controlled titanium (IV) oxide nanoparticles with co-catalyst loading. *Curr. Org. Chem.* **2013**, *17*, 2449–2453. [CrossRef]
111. Zaleska, A. Doped-TiO_2: A review. *Recent Pat. Eng.* **2008**, *2*, 157–164. [CrossRef]
112. Linsebigler, A.L.; Lu, G.; Yates, J.T. Photocatalysis on TiO_2 Surfaces: Principles, Mechanisms, and Selected Results. *Chem. Rev.* **1995**, *95*, 735–758. [CrossRef]
113. Liu, E.; Qi, L.; Bian, J.; Chen, Y.; Hu, X.; Fan, J.; Liu, H.; Zhu, C.; Wang, Q. A facile strategy to fabricate plasmonic Cu modified TiO_2 nano-flower films for photocatalytic reduction of CO_2 to methanol. *Mater. Res. Bull.* **2015**, *68*, 203–209. [CrossRef]
114. Kemp, T.J.; McIntyre, R.A. Transition metal-doped titanium (IV) dioxide: Characterisation and influence on photodegradation of poly (vinyl chloride). *Polym. Degrad. Stab.* **2006**, *91*, 165–194. [CrossRef]
115. Feng, H.; Zhang, M.-H.; Yu, L.E. Hydrothermal synthesis and photocatalytic performance of metal-ions doped TiO_2. *Appl. Catal. A* **2012**, *413–414*, 238–244. [CrossRef]
116. Di Valentin, C.; Pacchioni, G. Trends in non-metal doping of anatase TiO_2: B, C, N and F. *Catal. Today* **2013**, *206*, 12–18. [CrossRef]
117. Marschall, R.; Wang, L. Non-metal doping of transition metal oxides for visible-light photocatalysis. *Catal. Today* **2014**, *225*, 111–135. [CrossRef]
118. Sun, L.; Zhao, X.; Cheng, X.; Sun, H.; Li, Y.; Li, P.; Fan, W. Evaluating the C, N, and F pairwise codoping effect on the enhanced photoactivity of ZnWO4: The charge compensation mechanism in donor–acceptor pairs. *J. Phys. Chem. C* **2011**, *115*, 15516–15524. [CrossRef]
119. Wang, W.; Serp, P.; Kalck, P.; Silva, C.G.; Faria, J.L. Preparation and characterization of nanostructured MWCNT-TiO_2 composite materials for photocatalytic water treatment applications. *Mater. Res. Bull.* **2008**, *43*, 958–967. [CrossRef]
120. Oh, W.-C.; Zhang, F.-J.; Chen, M.-L. Preparation of MWCNT/TiO_2 composites by using MWCNTs and Titanium (IV) alkoxide precursors in Benzene and their photocatalytic effect and bactericidal activity. *Bull. Korean Chem. Soc.* **2009**, *30*, 2637–2642.
121. Kuo, C.-Y. Prevenient dye-degradation mechanisms using UV/TiO_2/carbon nanotubes process. *J. Hazard. Mater.* **2009**, *163*, 239–244. [CrossRef] [PubMed]
122. Wang, W.; Serp, P.; Kalck, P.; Faria, J.L. Photocatalytic degradation of phenol on MWNT and titania composite catalysts prepared by a modified sol–gel method. *Appl. Catal. B* **2005**, *56*, 305–312. [CrossRef]
123. Hu, G.; Meng, X.; Feng, X.; Ding, Y.; Zhang, S.; Yang, M. Anatase TiO_2 nanoparticles/carbon nanotubes nanofibers: Preparation, characterization and photocatalytic properties. *Asian J. Mater. Sci.* **2007**, *42*, 7162–7170. [CrossRef]
124. Aryal, S.; Kim, C.K.; Kim, K.-W.; Khil, M.S.; Kim, H.Y. Multi-walled carbon nanotubes/TiO_2 composite nanofiber by electrospinning. *Mater. Sci. Eng. C* **2008**, *28*, 75–79. [CrossRef]
125. Yu, H.; Quan, X.; Chen, S.; Zhao, H. TiO_2− multiwalled carbon nanotube heterojunction arrays and their charge separation capability. *J. Phys. Chem. C* **2007**, *111*, 12987–12991. [CrossRef]
126. Chen, M.-L.; Zhang, F.-J.; Oh, W.-C. Synthesis, characterization, and photocatalytic analysis of CNT/TiO_2 composites derived from MWCNTs and titanium sources. *New Carbon Mater.* **2009**, *24*, 159–166. [CrossRef]
127. Tang, B.; Chen, H.; Peng, H.; Wang, Z.; Huang, W. Graphene modified TiO_2 composite photocatalysts: Mechanism, progress and perspective. *Nanomaterials* **2018**, *8*, 105. [CrossRef]
128. Xiang, Q.; Yu, J.; Jaroniec, M. Graphene-based semiconductor photocatalysts. *Chem. Soc. Rev.* **2012**, *41*, 782–796. [CrossRef] [PubMed]

129. Chowdhury, S.; Balasubramanian, R. Graphene/semiconductor nanocomposites (GSNs) for heterogeneous photocatalytic decolorization of wastewaters contaminated with synthetic dyes: A review. *Appl. Catal. B* **2014**, *160*, 307–324. [CrossRef]
130. Jianwei, C.; Jianwen, S.; Xu, W.; Haojie, C.; Minglai, F. Recent progress in the preparation and application of semiconductor/graphene composite photocatalysts. *Chin. J. Catal.* **2013**, *34*, 621–640.
131. Singh, V.; Joung, D.; Zhai, L.; Das, S.; Khondaker, S.I.; Seal, S. Graphene based materials: Past, present and future. *Prog. Mater Sci.* **2011**, *56*, 1178–1271. [CrossRef]
132. Hu, C.; Lu, T.; Chen, F.; Zhang, R. A brief review of graphene–metal oxide composites synthesis and applications in photocatalysis. *J. Chin. Adv. Mater. Soc.* **2013**, *1*, 21–39. [CrossRef]
133. Ozer, L.Y.; Garlisi, C.; Oladipo, H.; Pagliaro, M.; Sharief, S.A.; Yusuf, A.; Almheiri, S.; Palmisano, G. Inorganic semiconductors-graphene composites in photo(electro)catalysis: Synthetic strategies, interaction mechanisms and applications. *J. Photochem. Photobiol. C* **2017**, *33*, 132–164. [CrossRef]
134. Wang, L.-Q.; Wang, D.; Liu, J.; Exarhos, G.J. Probing Porosity and Pore Interconnectivity in Self-Assembled TiO_2–Graphene Hybrid Nanostructures Using Hyperpolarized 129Xe NMR. *J. Phys. Chem. C* **2012**, *116*, 22–29. [CrossRef]
135. Ying, J.; Yang, X.-Y.; Tian, G.; Janiak, C.; Su, B.-L. Self-assembly: An option to nanoporous metal nanocrystals. *Nanoscale* **2014**, *6*, 13370–13382. [CrossRef]
136. Yu, X.; Lin, D.; Li, P.; Su, Z. Recent advances in the synthesis and energy applications of TiO_2-graphene nanohybrids. *Sol. Energy Mater. Sol. Cells* **2017**, *172*, 252–269. [CrossRef]
137. Kim, I.Y.; Lee, J.M.; Kim, T.W.; Kim, H.N.; Kim, H.I.; Choi, W.; Hwang, S.J. A Strong Electronic Coupling between Graphene Nanosheets and Layered Titanate Nanoplates: A Soft-Chemical Route to Highly Porous Nanocomposites with Improved Photocatalytic Activity. *Small* **2012**, *8*, 1038–1048. [CrossRef] [PubMed]
138. Tu, W.; Zhou, Y.; Liu, Q.; Yan, S.; Bao, S.; Wang, X.; Xiao, M.; Zou, Z. An In Situ Simultaneous Reduction-Hydrolysis Technique for Fabrication of TiO_2-Graphene 2D Sandwich-Like Hybrid Nanosheets: Graphene-Promoted Selectivity of Photocatalytic-Driven Hydrogenation and Coupling of CO_2 into Methane and Ethane. *Adv. Funct. Mater.* **2013**, *23*, 1743–1749. [CrossRef]
139. Tian, J.; Zhao, Z.; Kumar, A.; Boughton, R.I.; Liu, H. Recent progress in design, synthesis, and applications of one-dimensional TiO_2 nanostructured surface heterostructures: A review. *Chem. Soc. Rev.* **2014**, *43*, 6920–6937. [CrossRef] [PubMed]
140. Beigi, A.A.; Fatemi, S.; Salehi, Z. Synthesis of nanocomposite CdS/TiO_2 and investigation of its photocatalytic activity for CO_2 reduction to CO and CH_4 under visible light irradiation. *J. Co2 Util.* **2014**, *7*, 23–29. [CrossRef]
141. Li, X.; Liu, H.; Luo, D.; Li, J.; Huang, Y.; Li, H.; Fang, Y.; Xu, Y.; Zhu, L. Adsorption of CO_2 on heterostructure CdS(Bi_2S_3)/TiO_2 nanotube photocatalysts and their photocatalytic activities in the reduction of CO_2 to methanol under visible light irradiation. *Chem. Eng. J.* **2012**, *180*, 151–158. [CrossRef]
142. Wang, C.; Thompson, R.L.; Baltrus, J.; Matranga, C. Visible light photoreduction of CO_2 using CdSe/Pt/TiO_2 heterostructured catalysts. *J. Phys. Chem. Lett.* **2009**, *1*, 48–53. [CrossRef]
143. Wang, C.; Thompson, R.L.; Ohodnicki, P.; Baltrus, J.; Matranga, C. Size-dependent photocatalytic reduction of CO_2 with PbS quantum dot sensitized TiO_2 heterostructured photocatalysts. *J. Mater. Chem.* **2011**, *21*, 13452–13457. [CrossRef]
144. Asi, M.A.; He, C.; Su, M.; Xia, D.; Lin, L.; Deng, H.; Xiong, Y.; Qiu, R.; Li, X.-Z. Photocatalytic reduction of CO_2 to hydrocarbons using AgBr/TiO_2 nanocomposites under visible light. *Catal. Today* **2011**, *175*, 256–263. [CrossRef]
145. Kumar, S.; Isaacs, M.A.; Trofimovaite, R.; Durndell, L.; Parlett, C.M.; Douthwaite, R.E.; Coulson, B.; Cockett, M.C.; Wilson, K.; Lee, A.F. P25@ CoAl layered double hydroxide heterojunction nanocomposites for CO_2 photocatalytic reduction. *Appl. Catal. B* **2017**, *209*, 394–404. [CrossRef]
146. Low, J.; Yu, J.; Jaroniec, M.; Wageh, S.; Al-Ghamdi, A.A. Heterojunction photocatalysts. *Adv. Mater.* **2017**, *29*, 1601694. [CrossRef] [PubMed]
147. Li, H.; Zhou, Y.; Tu, W.; Ye, J.; Zou, Z. State-of-the-art progress in diverse heterostructured photocatalysts toward promoting photocatalytic performance. *Adv. Funct. Mater.* **2015**, *25*, 998–1013. [CrossRef]
148. George, S.M. Atomic layer deposition: An overview. *Chem. Rev.* **2010**, *110*, 111–131. [CrossRef] [PubMed]
149. Parsons, G.N.; George, S.M.; Knez, M. Progress and future directions for atomic layer deposition and ALD-based chemistry. *MRS Bull.* **2011**, *36*, 865–871. [CrossRef]

150. Lin, Y.; Xu, Y.; Mayer, M.T.; Simpson, Z.I.; McMahon, G.; Zhou, S.; Wang, D. Growth of p-type hematite by atomic layer deposition and its utilization for improved solar water splitting. *J. Am. Chem. Soc.* **2012**, *134*, 5508–5511. [CrossRef] [PubMed]
151. Wang, T.; Luo, Z.; Li, C.; Gong, J. Controllable fabrication of nanostructured materials for photoelectrochemical water splitting via atomic layer deposition. *Chem. Soc. Rev.* **2014**, *43*, 7469–7484. [CrossRef]
152. Son, D.H.; Hughes, S.M.; Yin, Y.; Paul Alivisatos, A. Cation exchange reactions in ionic nanocrystals. *Sci. (New York N.Y.)* **2004**, *306*, 1009–1012. [CrossRef]
153. Rivest, J.B.; Jain, P.K. Cation exchange on the nanoscale: An emerging technique for new material synthesis, device fabrication, and chemical sensing. *Chem. Soc. Rev.* **2013**, *42*, 89–96. [CrossRef]
154. Nguyen, T.-V.; Wu, J.C.S.; Chiou, C.-H. Photoreduction of CO_2 over Ruthenium dye-sensitized TiO_2-based catalysts under concentrated natural sunlight. *Catal. Commun.* **2008**, *9*, 2073–2076. [CrossRef]
155. Srikanth, B.; Goutham, R.; Badri Narayan, R.; Ramprasath, A.; Gopinath, K.P.; Sankaranarayanan, A.R. Recent advancements in supporting materials for immobilised photocatalytic applications in waste water treatment. *J. Environ. Manag.* **2017**, *200*, 60–78. [CrossRef]
156. Suárez, S. Immobilised Photocatalysts. In *Design of Advanced Photocatalytic Materials for Energy and Environmental Applications*; Coronado, J.M., Fresno, F., Hernández-Alonso, M.D., Portela, R., Eds.; Springer: London, UK, 2013; pp. 245–267. [CrossRef]
157. Wu, L.; Yang, D.; Fei, L.; Huang, Y.; Wu, F.; Sun, Y.; Shi, J.; Xiang, Y. Dip-Coating Process Engineering and Performance Optimization for Three-State Electrochromic Devices. *Nanoscale Res. Lett.* **2017**, *12*, 390. [CrossRef] [PubMed]
158. Kyesmen, P.I.; Nombona, N.; Diale, M. Influence of coating techniques on the optical and structural properties of hematite thin films. *Surf. Interfaces* **2019**, *17*, 100384. [CrossRef]
159. Deepa, M.; Saxena, T.K.; Singh, D.P.; Sood, K.N.; Agnihotry, S.A. Spin coated versus dip coated electrochromic tungsten oxide films: Structure, morphology, optical and electrochemical properties. *Electrochim. Acta* **2006**, *51*, 1974–1989. [CrossRef]
160. Matsushima, T.; Inoue, M.; Fujihara, T.; Terakawa, S.; Qin, C.; Sandanayaka, A.S.D.; Adachi, C. High-coverage organic-inorganic perovskite film fabricated by double spin coating for improved solar power conversion and amplified spontaneous emission. *Chem. Phys. Lett.* **2016**, *661*, 131–135. [CrossRef]
161. Pitoniak, E.; Wu, C.-Y.; Londeree, D.; Mazyck, D.; Bonzongo, J.-C.; Powers, K.; Sigmund, W. Nanostructured silica-gel doped with TiO_2 for mercury vapor control. *J. Nanopart. Res.* **2003**, *5*, 281–292. [CrossRef]